

Collaborative planning for power and hydrogen networks considering hydrogen pipeline slow dynamic and pipe storage characteristics

Guangyao Fan ^a, Wenchuan Zhang ^a, Haozeng Bie ^b, Xing Dong ^a, Ruicheng He ^a, Hui Zhang ^a, Fan Li ^a, Bo Sun ^{a,*}, Fengwen Pan ^{c,d}

^a School of Control Science and Engineering, Shandong University, Jinan, Shandong, 250061, China

^b School of Mechanical, Electrical & Information Engineering, Shandong University, Weihai, Shandong, 264209, China

^c National Center of Technology Innovation for Fuel Cell, Weifang, 261000, China

^d Weichai Power Co., Ltd, Weifang, 261061, China

ARTICLE INFO

Handling Editor: Dr M Mahdi Najafpour

Keywords:

Hydrogen network
Collaborative planning
Hydrogen pipeline
Power network
Benders algorithm

ABSTRACT

The coupling of the power network (PN) and hydrogen network (HN) can facilitate the consumption of renewable energy and promote the low-carbon transformation of the energy system. However, independent planning methods for PN or HN overlook the electricity-hydrogen inherent coupling and complementary properties, failing to meet the requirements of integrated collaborative planning. Furthermore, the storage potential of hydrogen pipelines is frequently overlooked in current planning frameworks. Therefore, a hydrogen pipeline model that considers the slow dynamic characteristics and pipe storage characteristics is firstly established. On this basis, a collaborative planning model for the PN and HN is established. Secondly, the planning problem is decomposed into an equipment siting capacity optimization master problem and an operation optimization sub-problem, and a solution method combining the Benders algorithm and the tabu search algorithm is proposed, which achieves the cyclic iterative solution by constructing the Benders cut. Finally, the effectiveness of the model and the collaborative planning method are validated using the examples of IEEE 5-node system (7-node hydrogen system) and IEEE 30-node system (20-node hydrogen system). The results show that the capacity of the hydrogen storage tank is reduced by 1.128 MW (31.7 %) by considering the dynamic modeling of the hydrogen pipeline in the planning. The total cost of the collaboratively planned the PN and HN is reduced by 17.06 % compared to the separate planning.

1. Introduction

1.1. Background and motivation

Hydrogen energy, a secondary energy source, has the advantages of cleaning, effectiveness and multiple application scenarios. It can accelerate the decarbonization of industry, building, transport and other sectors [1]. Up to now, more than 50 countries and regions have incorporated hydrogen energy into their energy development strategies. China has also issued a series of policies to vigorously promote the development of the hydrogen energy industry, stating that "Hydrogen energy is an important part of the future national energy system, and an important carrier for the realization of green and low-carbon transformation of energy end-use application" [2].

The power network (PN) and hydrogen network (HN) have

complementary advantages. Solar and wind energy can be converted into hydrogen through water electrolysis technology, facilitating large-scale consumption of renewable energy sources [3]. Fuel cells can convert hydrogen energy into electricity, improving the quality and reliability of power supply [4]. The power system can transmit energy over long distances, and hydrogen pipelines with storage characteristics can help to relieve the pressure of the power system at lower voltage levels, with almost zero energy loss [5]. Therefore, integrating the HN with the PN has become an important way to realize the green and low-carbon transformation of the energy system. In view of these advantages, there is an urgent requirement for collaborative planning and design of the PN and HN.

* Corresponding author.

E-mail address: sunbo@sdu.edu.cn (B. Sun).

1.2. Literature review

Currently, there are many studies that plan the PN and HN separately. In terms of the power system, its planning is aimed at upgrading the system to meet high renewable energy penetration and growing electricity demand, while coping with the technical and security constraints of the power grid [6]. Ref. [7] proposed an integrated planning model for generation, transmission and storage that considers short-term and long-term uncertainties. The model was a large-scale multi-stage stochastic mixed integer planning problem. Ref. [8] presented a new approach to wind and photovoltaic capacity expansion planning that considers frequency regulation capacity at the planning stage. This method facilitated the joint optimization of long-term capacity planning and short-term operational strategies, while maintaining frequency security constraints. The results show that an increase of about 13 % in renewable energy capacity is required to provide sufficient frequency regulation reserves and power supply. A two-stage unit expansion and generation planning model was proposed in Ref. [9], integrating the impact of generation technologies and policy directions on power system planning. The application value of the model in power system planning for 2020–2050 was investigated using an improved 40-node power system as an example. Ref. [10] suggested a short-term and seasonal energy storage planning method for renewable energy sources to achieve multi-temporal adequacy balancing of renewable energy sources. The findings demonstrated that the planning methodology achieves multi-timescale adequacy balancing in high renewable energy power systems and improves the economy of the planning system. In power system planning, power-to-heat, power-to-gas, power-to-hydrogen, etc. were often considered as a load, which was particularly important for the planning of large-capacity power systems with a high share of renewable energy generation [11,12].

In terms of the planning of the HIN, the planning model was developed in Ref. [13] considering hydrogen demand, renewable energy capacity, sources of electricity supply, levelized cost of hydrogen production and technology choice. Ref. [14] constructed a coupled co-ordinated planning model of resource availability, project distribution, and user requirements, and studied the spatial and temporal dynamics of the HIN. Ref. [15] provided a comprehensive multi-cycle model for hydrogen expansion planning, covering production to distribution. The model was used to optimize the timing, location, type and capacity of facilities while considering effective operational strategies. The results indicated that the levelized cost of hydrogen would be reduced to 3.89 USD/kg through the expansion plan. A multi-period urban hydrogen supply system siting and capacity planning framework based on multi-objective optimization of the HIN was proposed in Ref. [16], which was solved by using the third-generation non-dominated sequential genetic algorithm.

The coupling of the PN with other infrastructures such as heat and gas networks has attracted a lot of attention. Ref. [17] developed a two-layer optimization model for low carbon planning of integrated power and heat systems, enabling coordination between the system and its upstream network. And the precise carbon emissions of the system are tracked through the carbon flows of components, PNs and district heating networks. The joint security-constrained extended planning model for an integrated system of electricity and natural gas networks was proposed in Ref. [18], which was robust to uncertainty in load demand and wind power to ensure the system can withstand N-1 contingencies that may occur on a transmission line or a natural gas pipeline. Ref. [19] proposed an N-1 security constrained optimal power and gas flow framework incorporating a bi-directional gas flow model with an iterative algorithm to identify a subset of constraining events to ensure the manageability and effectiveness of the model. A unified planning approach that accounted for cascading interactions between the power and natural gas systems was proposed in Ref. [20]. A streamlined analytical framework was applied to derive the optimal planning strategy and simplify computational challenges. The proposed

model was tested on a combined natural gas and power system to validate its effectiveness. Ref. [21] established an energy network for rail transportation systems coupled with power, gas, and heat networks, and proposed a cooperative planning model for full life-cycle economic security.

With the development of hydrogen energy industry, the collaborative planning of PN and HN has gradually attracted the interest of researchers. Ref. [22] focused on establishing a mathematical model of large-scale hydrogen production via electrolysis, and constructed a planning model for the PN and HN that considered the fluctuation of renewable energy, and designed a decomposition algorithm based on dynamic planning to solve this problem. A collaborative planning model for PN and HN considering transportable seasonal hydrogen storage was proposed in Ref. [23], and the optimal configuration and operation of the system were investigated. The validity of the model was verified using the 5-bus PJM system and the HRP-38 system in the Northwest Region as examples. Ref. [24] innovatively developed a trading framework for coupled PN and hydrogen trailer transportation road network considering time delays and service continuity. Ref. [25] constructed collaborative planning models for PN and HN. The investment in system assets and renewable energy were optimized to meet the growing electricity load and the hydrogen electrolysis load. For the hydrogen energy system, hydrogen production, pipeline trailer transport and storage constraints were considered, and the capacity for hydrogen electrolysis and hydrogen storage was determined to be optimal to meet the hydrogen load. The case study demonstrated that the collaborative planning approaches can reduce the overall planning cost and promote the use of renewable energy.

In summary, there are many studies that planned the PN and HN separately. However, the coupling between them was rarely considered. In the above studies of collaborative planning of the PN and HN, hydrogen pipelines are modeled by Weymouth steady state model, and the dynamic characteristics of the pipeline are neglected, which limits the accurate description of the pipeline operation characteristics. Compared to steady state modeling, dynamic modeling based on fluid dynamics has important implications for energy systems, as it can accurately calculate the flow rate and pressure of the hydrogen pipeline and improve the operation efficiency of the energy system [26]. It is economically valuable to consider the storage characteristics of the hydrogen pipeline, which leads to higher operation flexibility, lower operation costs, and reduced wind power curtailment in the energy system [31]. In addition, ignoring the slow dynamics and pipe storage characteristics of the hydrogen pipeline in the collaborative planning of PN and HN could lead to irrational equipment configurations, and deficiencies in the economics and operation flexibility of the planning scheme.

1.3. Contributions

To fill the above gap, a dynamic model of hydrogen pipeline is established in this paper to conduct collaborative planning research for PN and HN. The innovations and contributions of this study are summarized as follows.

- (1) A hydrogen pipeline model that considers the slow dynamic characteristics and pipe storage characteristics comprehensively is established based on fluid dynamics principles. Compared with the traditional Weymouth steady state model, this model can accurately portray the operation characteristics of the hydrogen pipeline more consistent with the engineering reality, which can fully utilize the hydrogen storage potential of the pipeline and improve the economy of the planning scheme.
- (2) A collaborative planning model for siting-capacity-operation of the PN and HN considering economy, renewable energy penetration, and energy supply reliability is constructed. Compared to independent planning of PN and HN, this collaborative planning

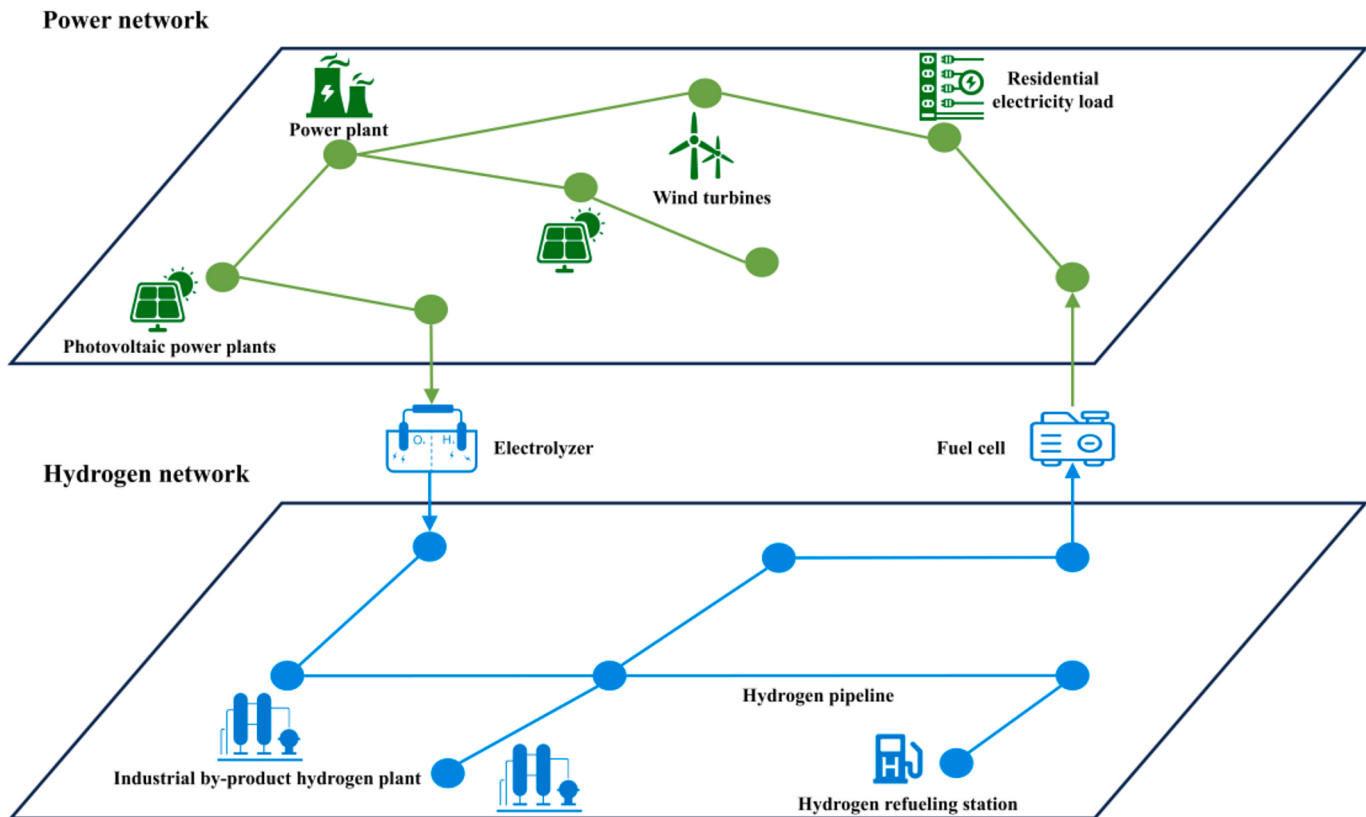


Fig. 1. The coupled structure of the PN and the HN.

model can capitalize on the complementary advantages of electric and hydrogen energy to promote joint economic development of the power and hydrogen sectors.

- (3) An efficient solution method for the planning model combining the Benders algorithm and the tabu search algorithm is proposed.
- (4) The effectiveness of the hydrogen pipeline dynamic model and the collaborative planning method are validated using the examples of IEEE 5-node system (7-node hydrogen system) and IEEE 30-node system (20-node hydrogen system).

2. Power and hydrogen networks

2.1. Structure

The coupled structure of the PN and HN is shown in Fig. 1. The power transmission network consists of power plant, wind turbines, photovoltaic power plants, power transmission lines and residential electric load. The HN consists of hydrogen energy supply plant, hydrogen pipeline and hydrogen refueling station. Industrial by-product hydrogen plant is selected as the hydrogen energy supply plant.

The hydrogen-electricity hybrid equipment includes hydrogen fuel

cells and the electrolyzer. Hydrogen fuel cells act as loads in the HN, using hydrogen as fuel to generate electricity and provide clean electricity for the PN. Electrolyzer act as loads in the PN, converting electric energy into hydrogen energy and providing a source of hydrogen for the HN. The hydrogen can either be supplied directly to the hydrogen load or delivered to the fuel cells for power generation, which effectively improves the energy supply reliability of the system.

2.2. Modelling

2.2.1. Hydrogen pipeline modelling

The modelling of the hydrogen pipeline and PN are based on different physics and have widely differing mechanism properties [27]. The inertia of the hydrogen pipeline is much larger than that of the PN, and the transient process of transitioning from one steady state to another is longer, with the regulation process typically being on the order of minutes to hours. At the same time, the hydrogen pipeline is able to store a certain amount of hydrogen, which is called ‘pipeline storage’ [28]. In previous studies, hydrogen pipelines were modeled using the traditional Weymouth steady state model, as shown in Section S1 of the Supplementary Material, which represents the relationship

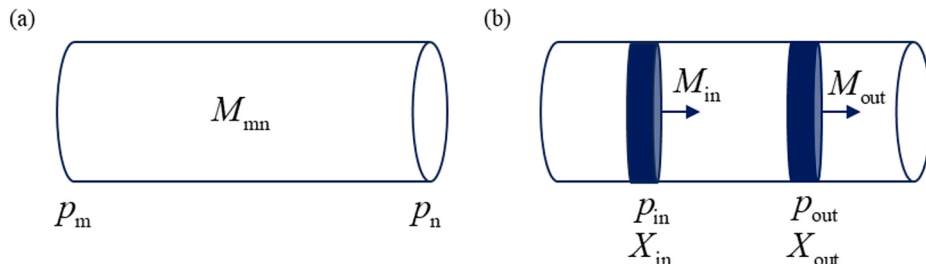


Fig. 2. Pipeline model. (a) Steady state model. (b) Discrete model.

between flow and pressure under steady state conditions (see Fig. 2 (a)), and is only suitable for pipeline calculations with constant flow and long-term stable operation [29]. In fact, the flow and pressure at each node of the hydrogen pipeline change with time, so to better meet the engineering reality, the following hydrogen pipeline model considering the slow dynamic and pipe storage characteristics is established.

(1) Dynamic model of the hydrogen pipeline

Hydrogen pipelines have the advantages of low losses, high hydrogen delivery and low cost, and is suitable for large-scale hydrogen delivery scenarios [30]. The dynamic characteristics of the gas flow in a pipeline are related to the diameter of the pipeline, the friction coefficient, and the gas pressure and temperature. It can be described by the flow continuity equation, the momentum equation, and the state equation.

The flow continuity equation is used to describe the conservation of mass of the gas in a pipeline. Disregarding the impact of external heat exchange, the equation can be expressed as.

$$\frac{\partial \rho}{\partial t} + \frac{\partial M}{\partial x} = 0 \quad (1)$$

where ρ is the density of hydrogen; t is the time; A is the pipeline cross-sectional area; x is the pipeline length; M is the hydrogen mass flow rate, can be expressed by the following equation.

$$M = \rho v A \quad (2)$$

where v is the hydrogen one-dimensional flow rate in the direction of the pipe.

The momentum equation describes the law of momentum transfer in a continuous gas. The one-dimensional form of this equation is shown below.

$$\frac{\partial(\rho v^2)}{\partial x} + \frac{\partial(\rho v)}{\partial t} + \frac{\partial p}{\partial x} + g\rho \sin \theta + \frac{\lambda}{d} \frac{v^2}{2} \rho = 0 \quad (3)$$

where p is the nodal gas pressure of hydrogen; g is the acceleration of gravity; θ is the angle between pipeline and level surface; λ is the pipeline friction coefficient; d is the diameter.

The state equation for the pipeline gas can be expressed as:

$$p = \rho c^2 \quad (4)$$

where c is the velocity of sound propagation in hydrogen, the expression is as follows:

$$c^2 = ZRT \quad (5)$$

where Z is the compression coefficient of hydrogen; R is the gas constant; T is the temperature.

The hydrogen pipeline dynamical modelling above takes the form of partial differential equations, which has obvious nonlinear characteristics. For this reason, the above model will be improved in this section to reduce the complexity of the solution while ensuring the accuracy of the model. In engineering practice, the pipeline gas flow velocity is much smaller than the sound velocity, and the convective inertia term $\partial(\rho v^2)/\partial x$ in the momentum equation (3) can be neglected. It is generally assumed that the hydrogen pipeline is laid horizontally and the angle θ between it and the horizontal plane is 0. The gravity term $g\rho \sin \theta$ is also 0 [31,32]. Based on the above simplification steps and substituting equation (2) into equation (3), it can be obtained.

$$\frac{\partial M}{\partial t} + \frac{\partial p}{\partial x} + \frac{\lambda v M}{2dA} = 0 \quad (6)$$

The time and space dependent partial differential terms described above are discretized using the finite difference method. The difference formulas used is shown below.

$$\frac{\partial X}{\partial t} = \frac{X_{out,t+1} + X_{in,t+1} - X_{out,t} - X_{in,t}}{2\Delta t} \quad (7)$$

$$\frac{\partial X}{\partial x} = \frac{X_{out,t+1} - X_{in,t+1}}{\Delta x} \quad (8)$$

$$X = \frac{X_{in,t+1} + X_{out,t+1}}{2} \quad (9)$$

where X_{in} is the state variable at the pipeline inlet; X_{out} is the state variable at the pipeline outlet; $t + 1$ is the next moment of t ; Δt and Δx respectively represent the time and space steps selected by the difference method. Since the research object is each section of the pipeline, the length of a single pipeline section l can be substituted for the spatial step Δx .

The original nonlinear partial differential equations can be discretized into algebraic equations by substituting equations (4), (7) and (8) into equation (1) and equations (7)–(9) into equation (6), respectively. The discretized model is shown in Fig. 2 (b). Finally, the nonlinear model is simplified to a linear model that is easy to solve computationally. The mass flow rate errors of the nonlinear and linear models are calculated with a single pipe, and the maximum error is only 3.12 %, which verifies the rationality of the simplified linear model.

$$\frac{1}{2c^2\Delta t} (p_{out,t+1} + p_{in,t+1} - p_{out,t} - p_{in,t}) + \frac{1}{lA} (M_{out,t+1} - M_{in,t+1}) = 0 \quad (10)$$

$$\begin{aligned} \frac{1}{2A\Delta t} (M_{out,t+1} + M_{in,t+1} - M_{out,t} - M_{in,t}) + \frac{1}{l} (p_{out,t+1} - p_{in,t+1}) \\ + \frac{\lambda}{4dA} (v_{out,t+1} M_{out,t+1} + v_{in,t+1} M_{in,t+1}) = 0 \end{aligned} \quad (11)$$

where p_{in} and p_{out} are inlet and outlet pressure of the pipe, respectively; M_{in} and M_{out} are the inlet and outlet mass flow rates, respectively; v_{in} and v_{out} are inlet and outlet one-dimensional flow rates, respectively.

(2) Pipe storage modeling of the hydrogen pipeline

From the above dynamic model, it can be seen that there is a certain delay and compressibility of hydrogen transmission in the pipeline, and a part of the gas will be retained in the pipeline, showing the pipe storage effect. According to the dynamic characteristics and the characteristics of hydrogen storage, the pipe storage model of the hydrogen pipeline is established.

$$\bar{M}_t |\bar{M}_t| + \left(\frac{\pi}{4} \right)^2 \frac{d^5}{\lambda c^2 l} (M_{out,t}^2 - M_{in,t}^2) = 0 \quad (12)$$

$$\frac{1}{l} (M_{out,t} - M_{in,t}) + \frac{\pi d^2}{4c^2 \Delta t} (\bar{p}_{t-1} - \bar{p}_t) = 0 \quad (13)$$

$$\begin{cases} \bar{M}_t = \frac{M_{in,t} + M_{out,t}}{2} \\ \bar{p}_t = \frac{p_{in,t} + p_{out,t}}{2} \end{cases} \quad (14)$$

where \bar{M}_t is the average hydrogen mass flow rate; \bar{p}_t is the average air pressure value in the pipeline.

From equation (12), it can be seen that there is a difference between the inlet and outlet gas flow rate, and this part is the pipe storage of the hydrogen pipeline, which can be expressed by the following equation.

$$Q_t = \frac{\pi d^2}{8c^2 \rho} (p_{in,t} + p_{out,t}) \quad (15)$$

where Q_t is the volume of hydrogen stored in the pipeline at the t moment.

In addition, the volume of gas stored in the pipe at the current time period is also related to the volume of gas in the pipe at the previous time

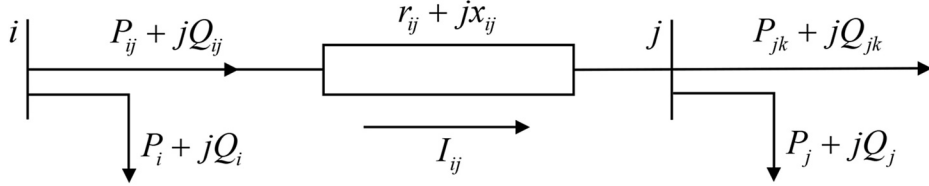


Fig. 3. Power flow model of the transmission network [33].

period by the following relationship.

$$Q_t = Q_{t-1} + \frac{M_{in,t} - M_{out,t}}{\rho} \quad (16)$$

The pipe storage characteristics of the hydrogen pipeline can be described by equation (15) and equation (16).

2.2.2. PN modelling

The power flow model of the PN is shown in Fig. 3.

The power flow equations of the network include node power balance equations and transmission line voltage drop equations as shown below.

$$P_{j,t} = P_{ij,t} - r_{ij}I_{ij,t}^2 - \sum_{k:j \rightarrow k} P_{jk,t} \quad (17)$$

$$Q_{j,t} = Q_{ij,t} - x_{ij}I_{ij,t}^2 - \sum_{k:j \rightarrow k} Q_{jk,t} \quad (18)$$

$$U_{j,t}^2 = U_{i,t}^2 - 2(r_{ij}P_{ij,t} + x_{ij}Q_{ij,t}) + (r_{ij}^2 + x_{ij}^2)I_{ij,t}^2 \quad (19)$$

$$I_{ij,t}^2 = \frac{P_{ij,t}^2 + Q_{ij,t}^2}{U_{i,t}^2} \quad (20)$$

where P and Q are the active and reactive power, respectively; r and x are the resistance and reactance, respectively; I is the current flowing; $k:j \rightarrow k$ represents that the power flow of the line jk is from node j to node k ; U is the voltage.

Due to the presence of square terms in the above power flow equations, it is impossible to apply the traditional numerical solution methods directly, and the strong nonlinearity and nonconvexity of the model bring great difficulties in solving the optimization problem. For this reason, it is first mathematically deformed such that:

$$\alpha_{i,t} = U_{i,t}^2 \quad (21)$$

$$\beta_{ij,t} = I_{ij,t}^2 \quad (22)$$

where $\alpha_{i,t}$ is the square of node i voltage value; $\beta_{ij,t}$ is the square of the current flowing.

By substituting equations (21) and (22) into equations (17)–(20), it can be obtained:

$$P_{j,t} = P_{ij,t} - r_{ij}\beta_{ij,t} - \sum_{k:j \rightarrow k} P_{jk,t} \quad (23)$$

$$Q_{j,t} = Q_{ij,t} - x_{ij}\beta_{ij,t} - \sum_{k:j \rightarrow k} Q_{jk,t} \quad (24)$$

$$\alpha_{j,t} = \alpha_{i,t} - 2(r_{ij}P_{ij,t} + x_{ij}Q_{ij,t}) + (r_{ij}^2 + x_{ij}^2)\beta_{ij,t} \quad (25)$$

$$\beta_{ij,t} = \frac{P_{ij,t}^2 + Q_{ij,t}^2}{\alpha_{i,t}} \quad (26)$$

The above power flow equations can then be turned into an easily solvable second-order cone planning problem by means of the second-order cone relaxation method [34]. The standard form of second-order

cone planning is shown below:

$$\min \{c^T x | Ax = b, x_i \in K, i = 1, 2, \dots, N\} \quad (27)$$

where variable $x \in R_N$; coefficient $b \in R_M$; coefficient $c \in R_N$; A is the coefficient matrix; $A_{M \times N} \in R_{M \times N}$.

Perform a second-order cone relaxation of equation (26) to obtain:

$$\beta_{ij,t} \geq \frac{P_{ij,t}^2 + Q_{ij,t}^2}{\alpha_{i,t}} \quad (28)$$

At this point, equation (28) satisfies the standard second-order cone transformation form and can be equivalently replaced by:

$$\left\| \begin{array}{l} 2P_{ij,t} \\ 2Q_{ij,t} \\ \beta_{ij,t} - \alpha_{i,t} \end{array} \right\|_2 \leq \beta_{ij,t} + \alpha_{i,t} \quad (29)$$

The second-order cone planning model of the power system consists of equations (23)–(25) and (29). The second-order cone relaxation error is calculated according to Ref. [32], and the maximum error is on the order of 10^{-6} , which meets the accuracy requirement, proving the effectiveness and accuracy of the second-order cone relaxation method.

2.2.3. Hydrogen-electricity hybrid device modelling

(1) Electrolyzer

The amount of hydrogen produced in the electrolyzer is calculated as follows [35].

$$P_{ETH_2,t} = \eta_{ETH_2,t} \times P_{ET,t} \quad (30)$$

where $P_{ETH_2,t}$ is the output power, kW; $P_{ET,t}$ is the input power, kW; $\eta_{ETH_2,t}$ is the efficiency of the electrolyzer.

(2) Fuel cell

The fuel cell is a highly promising and environmentally friendly energy conversion equipment. Its mathematical model is shown below [36].

$$P_{FC} = W_{H_2} \times \eta_{FC} \times LHV \quad (31)$$

where P_{FC} is the generated electric power; W_{H_2} is the hydrogen input rate; η_{FC} is the efficiency; LHV is the lower heating value of hydrogen.

3. Collaborative planning model for the PN and HN

3.1. Equipment siting and capacity planning master problem

3.1.1. Decision variables

The decision variables of the master problem consist of the installed nodes and capacity of the equipment which are shown as follows.

$$\begin{aligned} X_1 &= [N_{11} \dots N_{1m}, R_{11} \dots R_{1m}] \\ X_2 &= [N_{21} \dots N_{2m}, R_{21} \dots R_{2m}] \\ &\vdots \\ X_n &= [N_{n1} \dots N_{nm}, R_{n1} \dots R_{nm}] \end{aligned} \quad (32)$$

where n is the number of equipment, m is the number of nodes, N_{11}, \dots, N_{nm} represent the 0–1 variables of the equipment candidate nodes, R_{11}, \dots, R_{nm} represent the equipment capacity variables corresponding to the candidate nodes.

3.1.2. Objective function

The total cost includes the annual equipment investment cost, the operation cost, and the carbon emission cost. Therefore, the objective function is to minimize the total cost [37].

$$\min C = \min(C_{inv} + C_{ope} + C_{em}) = \min(C_{inv} + C_{sp}) \quad (33)$$

where C is the total cost, C_{inv} is the investment cost, C_{ope} is the operation cost; C_{em} is the carbon emission cost. C_{sp} is the objective function of the subproblem.

The investment cost is calculated as follows.

$$C_{inv} = \sum_{k=1}^n \left[c_k R_k \cdot \frac{dr(1+dr)^{\tau_k}}{(1+dr)^{\tau_k} - 1} \right] \quad (34)$$

where c_k is the investment cost per unit capacity of the k equipment; R_k is the installation capacity of the k equipment; dr is the discount rate; τ_k is the life.

3.1.3. Constraints

Renewable energy devices and the hydrogen-electricity hybrid devices are required to meet the following constraints.

$$R_{WT,min} \leq R_{WT} \leq R_{WT,max} \quad (35)$$

$$R_{PV,min} \leq R_{PV} \leq R_{PV,max} \quad (36)$$

$$R_{ET,min} \leq R_{ET} \leq R_{ET,max} \quad (37)$$

$$R_{FC,min} \leq R_{FC} \leq R_{FC,max} \quad (38)$$

where the subscripts max and min represent the maximum and minimum installed capacity of the equipment, respectively.

3.2. Operation optimization subproblem

3.2.1. Decision variables

The decision variables of the operation optimization subproblem is the output of each equipment.

3.2.2. Objective function

The objective function of the operation optimization subproblem is to minimize the sum of the operation cost and the carbon cost of the system, as shown below.

$$\min C_{sp} = \min(C_{ope} + C_{em}) \quad (39)$$

$$C_{ope} = C_{om} + C_{pur} \quad (40)$$

where C_{om} is the operation and maintenance cost; C_{pur} is the energy purchase cost. The calculation formula is shown below.

$$C_{om} = \sum_{k=1}^n c_{om,k} \sum_{t=1}^{8760} P_{k,t} \quad (41)$$

$$C_{pur} = \sum_{t=1}^{8760} (c_{TG,t} P_{TG,t} + c_{H_2} M_{H_2,t}) \quad (42)$$

where $c_{om,k}$ is the unit operation and maintenance cost; $P_{k,t}$ is the power of the k equipment at the t moment; $c_{TG,t}$ is the unit price of electricity generated by traditional power plants at the t moment; $P_{TG,t}$ is the power generation of traditional power plants; c_{H_2} is the unit price of purchased

hydrogen; $M_{H_2,t}$ is the amount of hydrogen purchased at the t moment.

The carbon emission cost is calculated by the following formula.

$$C_{em} = \xi_{carb} \sum_{t=1}^{8760} \lambda_e \cdot P_{TG,t} \quad (43)$$

where ξ_{carb} is the unit carbon emission cost; λ_e is the carbon emission per unit of electricity generated by power plant.

3.2.3. Constraints

The constraints for the operation optimization of the PN and HN are as follows.

(1) Hydrogen pipeline constraints

The dynamic characteristic constraints and pipe storage constraints for the hydrogen pipeline are shown in equations (10), (11), (15) and (16) in Section 2.2.1.

To ensure the safe operation, the pressure at each node in the hydrogen pipeline should have its upper and lower limits, constrained as follows [38].

$$p_{i,min} \leq p_{i,t} \leq p_{i,max} \quad (44)$$

where $p_{i,t}$ is the pressure of the i node at the t moment; $p_{i,max}$ and $p_{i,min}$ are upper and lower pressure limits, respectively.

At the same time, the hydrogen flow rate transmitted by the pipeline cannot exceed the upper limit of the pipeline.

$$-M_{ij,max} \leq M_{ij,t} \leq M_{ij,max} \quad (45)$$

where $M_{ij,t}$ is the hydrogen flow rate of the pipeline ij ; $M_{ij,max}$ is the upper limit of hydrogen flow rate of the pipeline ij .

The nodes in the hydrogen pipeline also need to satisfy the flow balance constraint, i.e., the gas flow into each node should be equal to the gas flow out of that node, as shown below.

$$M_{HS_i,t} + M_{ET_i,t} - \sum_{j \in i} M_{ij,t} - M_{FC_i,t} - M_{L_i,t} = 0 \quad (46)$$

where $M_{HS_i,t}$ is the amount of hydrogen purchased by the node i from hydrogen supply plants at the t moment; $M_{ET_i,t}$ is the hydrogen production flow rate of the electrolyzer; $j \in i$ is all other nodes directly connected to the node i ; $M_{FC_i,t}$ is the flow rate of hydrogen supplied to the fuel cell by the node i at the t time. $M_{L_i,t}$ is the hydrogen load.

(2) PN constraints

The power flow constraints of the PN are shown in equations (23)–(25) and (29) in Section 2.2.2.

In a transmission network, the voltage at each node on the power line must not exceed the maximum and minimum values of the permit voltage.

$$U_{i,min}^2 \leq U_{i,t}^2 \leq U_{i,max}^2 \quad (47)$$

where $U_{i,t}$ is the voltage value; $U_{i,max}$ and $U_{i,min}$ are the maximum and minimum values of node voltage, respectively.

The transmission line cannot deliver more electric power than the upper limit, so there is the following constraint.

$$-P_{ij,max} \leq P_{ij,t} \leq P_{ij,max} \quad (48)$$

where $P_{ij,t}$ is the electric power; $P_{ij,max}$ is the upper limit of transmission power.

In addition, the nodes in the PN are required to satisfy the electric power balance constraint, i.e., the power flowing into each node must be equal to the power flowing out of that node, as shown below.

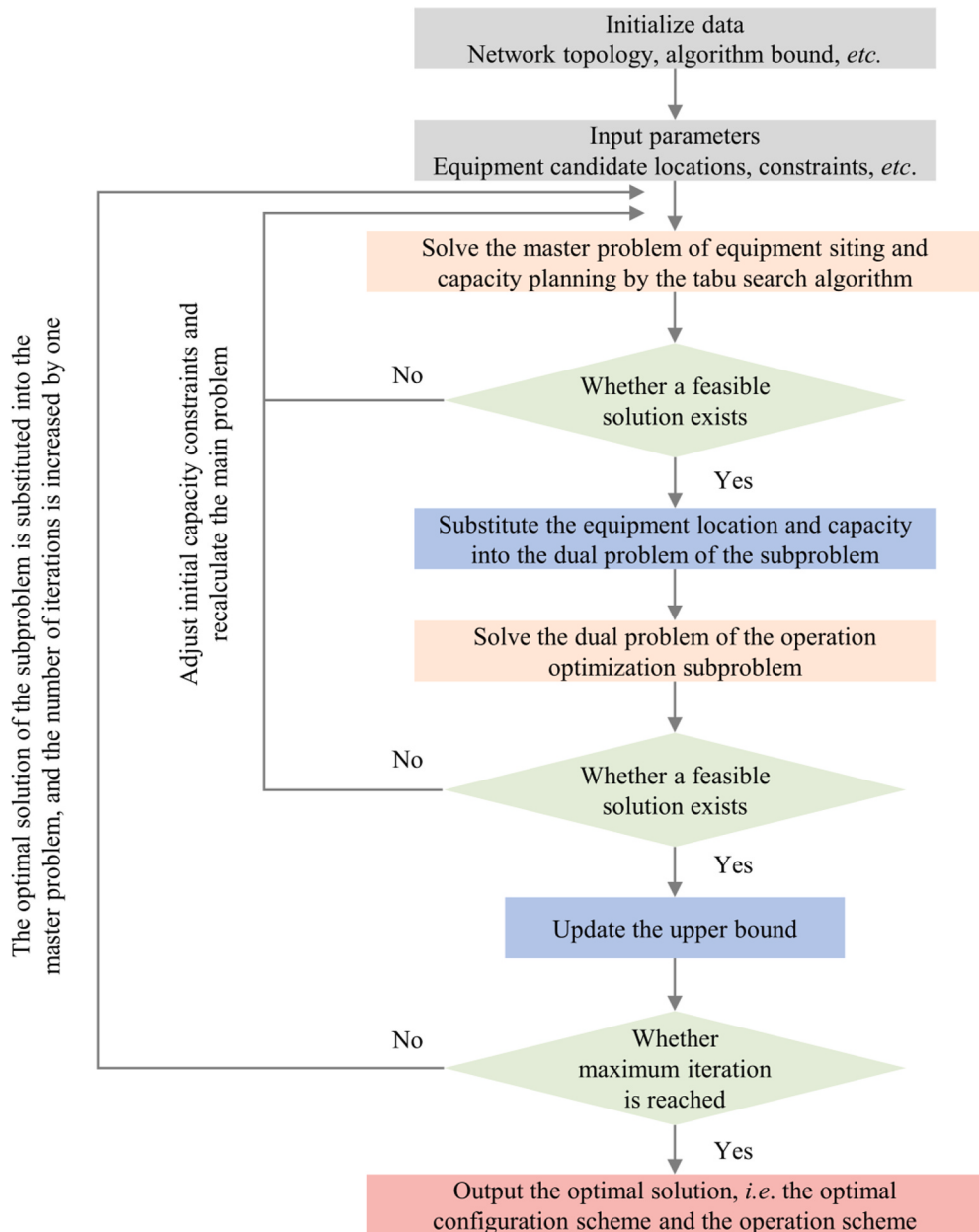


Fig. 4. The specific steps for solving the collaborative planning problem.

$$P_{grid,i,t} + P_{FC_i,t} + P_{WT_i,t} + P_{PV_i,t} - \sum_{j \in I} P_{ij,t} - P_{ET_i,t} - P_{L_i,t} = 0 \quad (49)$$

where $P_{grid,i,t}$ is the purchasing electricity from the grid of the node i at the t time; $P_{FC_i,t}$ is the fuel cell output; $P_{WT_i,t}$ is the wind turbine output; $P_{PV_i,t}$ is the photovoltaic power generation equipment output; $P_{ET_i,t}$ is the electrical power consumed of the electrolyzer; $P_{L_i,t}$ is the electric load.

(3) Hydrogen-electricity hybrid equipment constraints

The operation constraints of the electrolyzer and the fuel cell are shown below.

$$P_{ET,min} \leq P_{ET,t} \leq P_{ET,max} \quad (50)$$

$$P_{FC,min} \leq P_{FC,t} \leq P_{FC,max} \quad (51)$$

(4) Renewable energy generation equipment constraints

$$P_{WT,min} \leq P_{WT,t} \leq P_{WT,max} \quad (52)$$

$$P_{PV,min} \leq P_{PV,t} \leq P_{PV,max} \quad (53)$$

(5) Renewable energy permeability constraints

A high proportion of renewable energy generation is important for enhancing the environmental friendliness. Therefore, energy systems should focus on increasing the renewable energy permeability of the system during the planning process. In this section, renewable energy permeability is defined as the ratio of renewable energy generation to total system electricity supply, and the following constraints are placed on renewable energy permeability [39].

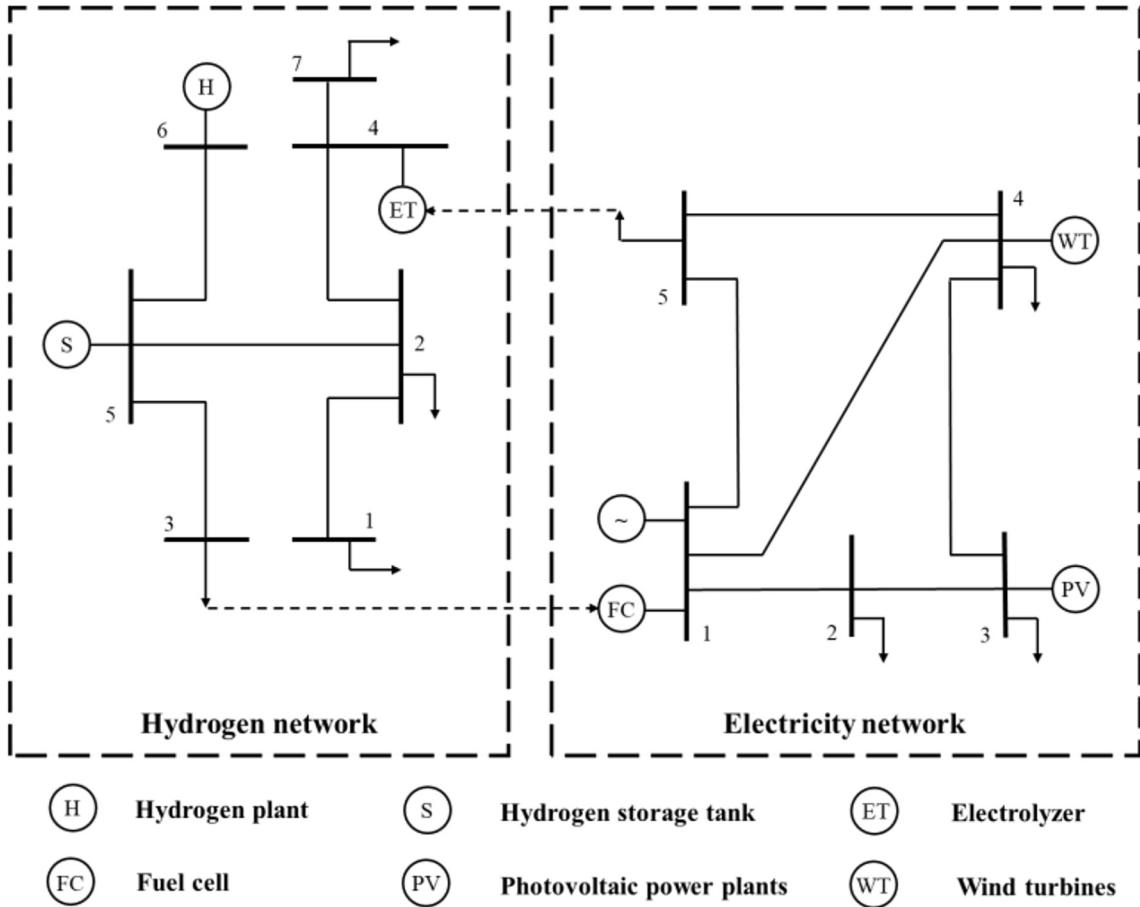


Fig. 5. IEEE 5-node system and 7-node hydrogen system topology structure map.

$$\delta_{OC} = \frac{\sum_{t=1}^{t_{\max}} (P_{WT,t} + P_{PV,t})}{\sum_{t=1}^{t_{\max}} (P_{TC,t} + P_{PC,t} + P_{WT,t} + P_{PV,t})} \cdot 100\% \geq \delta_{\min} \quad (54)$$

where δ_{\min} is the minimum value of the given renewable energy permeability.

(6) Energy supply reliability constraints

Energy supply reliability is the ability to continuously and stably meet the demand of energy loads during operation, which can be expressed by the energy supply reliability rate ψ . The system's supply reliability is evaluated by determining the adequacy of hydrogen and electric energy delivery to the load, and the following constraints on supply reliability are made [40].

$$\psi_e = \left\{ 1 - \frac{\max\{0, P_{eload,t} + P_{ET,t} - P_{WT,t} - P_{PV,t} - P_{FC,t}\}}{P_{eload,t} + P_{ET,t}} \right\} \cdot 100\% \geq \psi_{e,\min} \quad (55)$$

$$\psi_{H_2} = \left\{ 1 - \frac{\max\{0, M_{H_2load,t} + M_{FC,t} - M_{ET,t}\}}{M_{H_2load,t} + M_{FC,t}} \right\} \cdot 100\% \geq \psi_{H_2,\min} \quad (56)$$

where ψ_e and ψ_{H_2} are respectively the reliability of electric and hydrogen energy supply; $P_{eload,t}$ and $M_{H_2load,t}$ are respectively the electric and hydrogen load; $\psi_{e,\min}$ is the minimum value of power supply reliability; $\psi_{H_2,\min}$ is the minimum value of hydrogen supply reliability.

3.3. Solution algorithm

The planning problem for PN and HN is a large-scale mixed-integer planning problem. In order to solve such problems, the Benders decomposition algorithm proposed by J. F. Benders [41] is used. The variables are separated according to the model characteristics of the original complex problem, and the overall model is decomposed into the smaller and easy-to-solve master problem and subproblem based on the types of decision variables and constraints. In the collaborative planning problem, the master problem is the equipment siting and capacity planning of each equipment, which contains integer-type variables, and the subproblem is the operation optimization, which contains only continuous-type variables. Then the master and subproblem are related to each other by Benders cut constraints, and the master problem and subproblem are solved by loop iteration, which finally converge to the optimal solution of the original problem.

When using the Benders decomposition algorithm to solve the collaborative planning problem for the PN and HN, the master problem of investment decision for equipment is not only an integer planning problem but also an NP-hard problem. Meanwhile, during the iterative solving process, the subproblem continuously adds the newly generated Benders cut constraints to the master problem, and the scale of the whole problem is enlarged, which leads to a significant increase in the solving time of the master problem. At this time, the solving efficiency of the whole problem is mainly limited by the speed of solving the main problem. Therefore, the tabu search algorithm is introduced to enhance the efficiency of solving the master problem. The tabu search algorithm can efficiently obtain the approximate optimal solution of master problem, which can speed up the convergence of the whole algorithm. Compared with the traditional optimization algorithm, the tabu search

algorithm has better global search ability [42]. Set the tabu length $HL = 5$, the number of neighborhood solutions $Nb = 20$, and set the maximum number of iterations is 100. A sensitivity analysis of these parameters is performed, and the optimization results remain essentially unchanged when the parameters are larger than the set values, thus these set values are reasonable.

3.4. Solution process

The specific steps for solving the collaborative planning problem by the improved Benders hybrid tabu search algorithm are shown in Fig. 4.

- Step 1: Initialize data, including topology and parameters of PN and HN, hydrogen and electricity load at each node, economic and technical parameters of each equipment. Initialize the upper bound $UB = +\infty$ and lower bound $LB = -\infty$.
- Step 2: Input parameters such as candidate location and capacity constraints for electrolyzer, fuel cell, wind turbines, photovoltaic panels. Input technical parameters to form constraints.
- Step 3: Solve the master problem of equipment siting and capacity planning by the tabu search algorithm. The optimal solution of the master problem from the current iteration serves as the initial solution for the master problem in the subsequent iteration.
- Step 4: Judge whether a feasible solution exists for the master problem solved in step 3. If it exists, update the planning result of each equipment, and the match value obtained from the master problem is used as the lower bound LB , and go to step 5. Otherwise, reasonably adjust the system constraints according to the environment of the equipment installation site and other factors, and return to Step 3 to re-calculate the master problem.
- Step 5: Substitute the updated planning parameters as fixed values into the dual problem of the operation optimization subproblem, the dual problem is solved efficiently by calling the CPLEX solver in the YALMIP modelling environment, and then determine whether there is a bounded feasible solution. If there is a bounded feasible solution to the dual subproblem, Step 6 is executed; if the dual subproblem is unbounded, Step 7 is executed; if there is no solution to the dual subproblem, then the original problem does not have an optimal solution, and the initial parameters of the system need to be adjusted reasonably and solved again.
- Step 6: When a bounded feasible solution exists for the dual subproblem, update the upper bound UB and determine whether the number of consecutive unimproved times during the iteration process reaches a predetermined value. If yes, the collaborative planning problem for PN and HN obtains an optimal solution and goes to Step 8; otherwise, pass a subproblem optimality Benders cut constraint to the master problem and proceed to Step 3.
- Step 7: In the case where the dual subproblem is unbounded and there is no feasible solution to the subproblem, add a feasible Benders cut constraint to the master problem and return to Step 3.
- Step 8: Output the optimal solution to the PN and HN cooperative planning problem and the investment planning scheme.

4. Results and discussions

4.1. IEEE 5-node system and 7-node hydrogen system case study

4.1.1. Case description

IEEE 5-node system and 7-node hydrogen system are used as the first case study, two comparison scenarios are established and the planning results are compared. Scenario 1 is planned using a dynamic model of the hydrogen pipeline, i.e., considering the slow dynamics and pipe storage characteristics, and Scenario 2 is planned using the traditional Weymouth steady state model [29]. The topology is shown in Fig. 5. The wind turbines are located at node 4 of the PN, the photovoltaic units are located at node 3 of the PN, and node 1 of the PN is connected to a

Table 1

System planning scheme based on hydrogen pipeline dynamic modeling and Weymouth steady state modeling.

Planned equipment	Capacity (MW)	
	Scenario 1	Scenario 2
Wind turbines	8.592	8.335
Photovoltaic panels	6.861	6.693
Electrolyzer	4.127	4.276
Fuel cell	3.349	2.858
Hydrogen storage tank	2.433	3.561

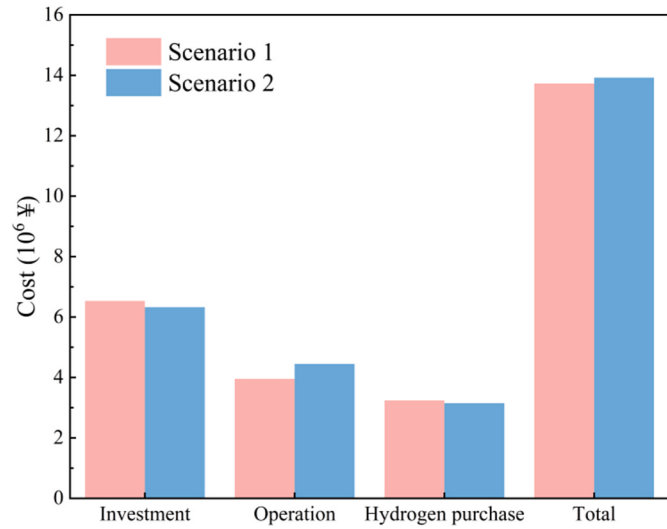


Fig. 6. Cost comparison of planning schemes based on hydrogen pipeline dynamic modeling and Weymouth steady state modeling.

superior power grid. The electrolyzer is installed between node 4 of the HN and node 5 of the PN, the fuel cell is installed between node 3 of the HN and node 1 of the PN, and the hydrogen storage is installed at node 5 of the HN (the mathematical model and parameter settings of the hydrogen storage tank are shown in Section S2 of the Supplementary Material). The capacity optimization of the above equipment is conducted.

4.1.2. Comparison of planning results

The configuration results of the two scenarios are shown in Table 1. The capacity of the hydrogen storage tank in Scenario 1 is significantly smaller than that in Scenario 2. This is due to the fact that the hydrogen pipeline model used in Scenario 1 considers the pipeline storage characteristics, and the hydrogen in the pipeline is used as a potential energy storage resource, which reduces the dependence on the hydrogen storage tank to a certain extent, and the capacity of the hydrogen storage tank is reduced by 1.128 MW (31.7%). The system is capable of adjusting the flow and storage of hydrogen according to real-time demand, thereby optimizing the distribution and utilization efficiency of hydrogen energy resources without adding additional hydrogen storage facilities. At the same time, the system's demand for additional hydrogen resources is reduced, leading to a decrease in the capacity of the electrolyzer in Scenario 1, by 0.149 MW, which reduces the investment cost of the electrolyzer. Scenario 1 is configured with larger capacity of renewable energy generation equipment and fuel cell.

The costs of the optimal planning schemes for Scenario 1 and Scenario 2 are shown in Fig. 6. The total cost of Scenario 1 is 13.727×10^6 ¥, which is reduced by 1.95×10^5 ¥ compared to Scenario 2. This is due to the fact that the system based on the pipeline dynamic model allows for load buffering by utilizing hydrogen storage in the pipeline when the demand for hydrogen is increasing, reduces the capacity of the hydrogen

Table 2

Output data for power plants.

Node	Rated power (MW)	Minimum power output (MW)	Power adjustment limit (MW)
1	200	50	50
2	80	0	30

storage tanks, increases the capacity of the renewable energy power generation equipment and the fuel cell, and reduces the purchased power from the superior grid, which effectively reduces the operation cost of the system by 4.91×10^5 ¥. In summary, planning based on traditional steady-state hydrogen pipeline model tends to lead to more conservative optimization results, which are not competitive in terms of total planning cost, while planning schemes considering slow dynamics and pipe storage characteristics of hydrogen pipelines are more economically advantageous.

4.2. IEEE 30-node system and 20-node hydrogen system case study

4.2.1. Case description

A system consisting of an improved IEEE 30-node system and a 20-node hydrogen system is used as a research object. First, the topology of the standard IEEE 30-node system is adapted to meet the energy transition needs. Several original conventional power plants are removed from the system to provide space for the introduction of the renewable power generation equipment and fuel cell units in the

planning study, which helps to improve the environmental friendliness and renewable energy penetration of the regional energy system. The output data of the modified power plant are shown in **Table 2**. The topology of the modified IEEE 30-node system is shown in **Fig. 7**, which contains 41 transmission lines and retains power plant only at nodes 1 and 2.

There are 21 load nodes in this PN and the load parameters of each node are shown in **Table 3**. The parameters of each branch in the topology are the same as the branch parameters of a standard IEEE 30-node system.

The topology of the 20-node hydrogen system is shown in **Fig. 8**, in which node 1, node 5, node 8, and node 14 access the hydrogen source

Table 3
PN load node parameters.

Load node	Power (MW)	Load node	Power (MW)
2	21.7	17	9.0
3	2.4	18	3.2
4	7.6	19	9.5
5	9.4	20	2.2
7	22.8	21	17.5
8	30.0	23	23.2
10	5.8	24	8.7
12	11.2	26	3.5
14	6.2	29	2.4
15	8.2	30	10.6
16	3.5	—	—

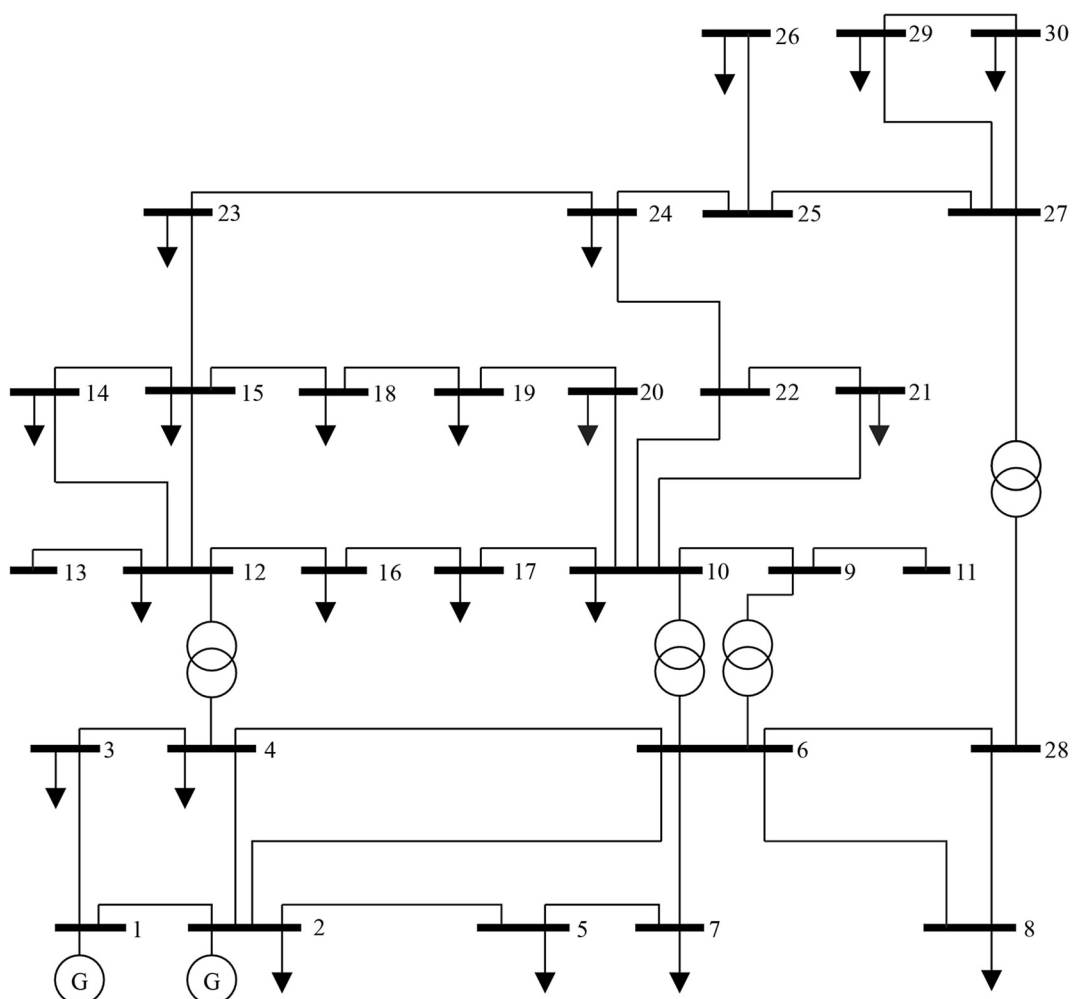


Fig. 7. IEEE 30-node system topology structure map.

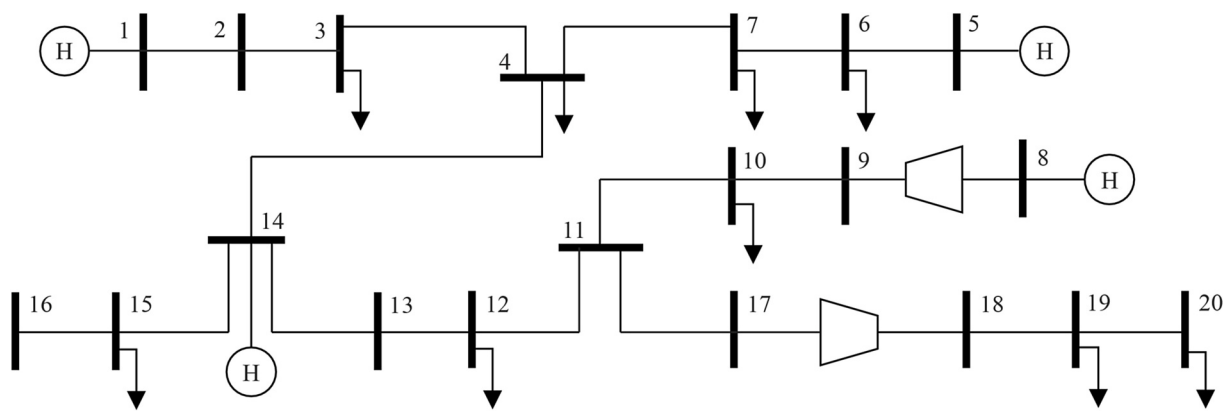


Fig. 8. 20-node hydrogen system topology structure map.

Table 4
HN node parameters.

HN node	Minimum pressure (bar)	Maximum pressure (bar)	HN node	Minimum pressure (bar)	Maximum pressure (bar)
1	0	77.0	11	0	66.2
2	0	77.0	12	0	66.2
3	30.0	80.0	13	0	66.2
4	0	80.0	14	0	66.2
5	0	77.0	15	0	66.2
6	30.0	80.0	16	30.0	66.2
7	30.0	80.0	17	0	66.2
8	0	66.2	18	0	80.0
9	0	66.2	19	0	66.2
10	30.0	66.2	20	25.0	66.2

from the hydrogen supply plant, and the HN contains 19 hydrogen transmission pipelines. The parameters of the nodes and pipelines in the HN are shown in Tables 4 and 5.

There are eight load nodes in this HN and the hydrogen load parameters of each node are shown in Table 6. The amount of hydrogen supplied and the cost of hydrogen supplied by each energy supply plant station in the HN are shown in Table 7.

When planning for the location of renewable energy power generation equipment, locations rich in wind and solar energy resources should be selected, and the land size limitations of the installation locations should be fully considered. According to the natural resource endowment of the planning area, the candidate installation locations for wind turbines and photovoltaic power generation equipment are node 5, node 8, node 11 and node 13 of the PN, and it is set that wind turbines and photovoltaic equipment should not be installed at the same time at the same node. To effectively cope with wind and light curtailment that may occur during renewable energy power generation, the source of power supply for the electrolysis cell should be the planned node of the renewable energy power generation plant. Therefore, the coupling

nodes of the electrolysis cell equipment and the PN should also be selected from node 5, node 8, node 11 and node 13. Meanwhile, considering the source-load distribution characteristics of the nodes in the HN, the candidate installation locations of the electrolyzer equipment are node 2, node 8, node 13 and node 14 of the HN. Based on the geographical distribution characteristics of the nodes in the PN and HN, the candidate installation locations for the hydrogen fuel cell are node 8, node 19, and node 23 of the PN; and the optional coupling nodes with the HN are node 9 and node 15. The output of the photovoltaic power plant and the wind turbine on a typical day is shown in Fig. 9. The relevant parameters of the equipment are given in Table 8.

Three different planning scenarios are set up.

Scenario 1: Collaborative planning of the PN and HN, considering the two-way coupling between hydrogen and electricity.

Scenario 2: The PN and HN are planned separately and

Table 6
HN load node parameters.

Load node	Hydrogen load (Mm ³)	Load node	Hydrogen load (Mm ³)
3	0.392	12	0.212
6	0.403	15	0.385
7	0.526	19	0.022
10	0.437	20	0.192

Table 7
Hydrogen supply data of the energy supply plants.

Node of the hydrogen energy supply plant	Minimum hydrogen supply (Mm ³)	Maximum hydrogen supply (Mm ³)	Unit cost (¥/m ³)
1	0	0.614	2.32
5	0	0.672	2.43
8	0.106	0.210	2.43
14	0.070	0.544	2.32

Table 5
HN pipeline parameters.

Pipeline number	Initial node	End node	Pipeline coefficient	Pipeline number	Initial node	End node	Pipeline coefficient
1	1	2	0.270	11	11	12	1.060
2	2	3	0.604	12	12	13	1.110
3	3	4	0.590	13	13	14	0.460
4	5	6	0.300	14	14	15	0.830
5	6	7	0.350	15	15	16	0.650
6	7	4	0.420	16	11	17	0.260
7	4	14	0.860	17	17	18	0.206
8	8	9	0.460	18	18	19	0.202
9	9	10	1.010	19	19	20	0.230
10	10	11	0.450	—	—	—	—

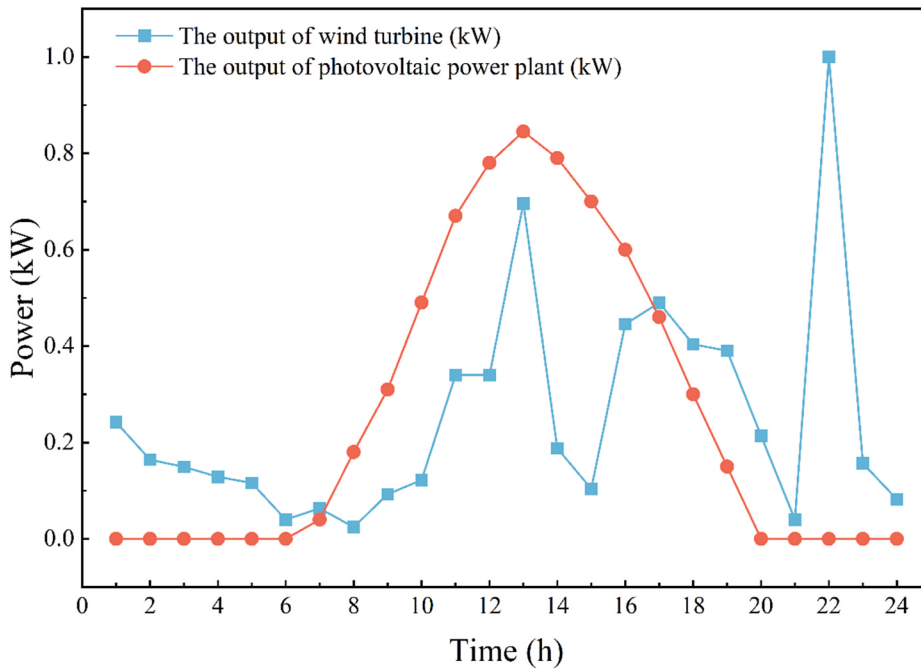


Fig. 9. The output of the photovoltaic power plant and the wind turbine on a typical day.

Table 8
The parameters of the equipment [43,44].

Parameter	Value
dr	0.05
τ	20 years
c_{WT}	4900 ¥/kW
$c_{om,WT}$	0.028 ¥/kWh
c_{PV}	3000 ¥/kW
$c_{om,PV}$	0.009 ¥/kWh
c_{ET}	2500 ¥/kW
$c_{om,ET}$	0.046 ¥/kWh
c_{FC}	4800 ¥/kW
$c_{om,FC}$	0.021 ¥/kWh

topology of the PN and HN after collaborative planning is shown in Fig. 10. Each planning equipment and coupling relationship is represented by red lines. The convergence and stability of the algorithm is verified in this case, as shown in Section S3 of the Supplementary Material.

The result of equipment siting and capacity for the system under Scenario 2 are presented in Table 10. The result of equipment siting and capacity of the system under Scenario 3 are shown in Table 11.

The total costs of the three scenarios are compared as described in Fig. 11. The lowest total planning cost of is achieved in Scenario 1, is 1.011×10^8 ¥, a reduction of 17.06 % (2.08×10^7 ¥) and 11.00 % (1.25×10^7 ¥) compared to Scenario 2 and Scenario 3, respectively, which indicates that the PN and HN complement each other, and the collaborative planning of both has economic advantages.

In particular, the investment cost of Scenario 1 is 4.755×10^7 ¥, which is significantly lower compared to Scenarios 2 and 3, by 35.6 % (2.632×10^7 ¥) and 22.8 % (1.405×10^7), respectively. In Scenario 2, since the coupling between hydrogen and electrical energy is not considered, and additional capacity of renewable energy generation equipment is required to meet the real-time load demand. The installed capacity of wind turbines and photovoltaic panels is 123.6 MW and 150.4 MW, respectively, an increase of 84.3 MW and 105.2 MW relative to Scenario 1. This leads to an increase in the annual investment cost. At the same time, there is a mismatch between renewable resources and electricity demand, which leads to a waste of renewable resources when renewable energy generation is more than demand because there is no hydrogen energy system to consume the excess electricity. The capacity of the wind turbine and photovoltaic panels in Scenario 3 is similar to that of Scenario 1. Although Scenario 3 is not equipped with electrolyzer, the capacity of the fuel cell is significantly increased and expensive, by 31.5 MW, which leads to an increase in the investment cost. The annual operation cost of the system includes the cost of power generation from the power plants, the carbon emission cost, and the cost of operation and maintenance of the other equipment. The operation and maintenance costs of the electrolyzer are higher, resulting in a slight increase in operation costs for Scenario 1. The electricity and hydrogen are complementary in Scenario 1, and the excess renewable electricity can be converted to hydrogen, reducing the need to purchase hydrogen from the hydrogen plant, so the hydrogen purchase cost for Scenario 1 is

Table 9
The results of collaborative planning for PN and HN.

Planned equipment	Node		Capacity (MW)
	PN	HN	
Wind turbines	Node 5	–	33.893
	Node 11	–	5.390
Photovoltaic panels	Node 13	–	45.270
	Node 5	Node 13	4.228
Electrolyzer	Node 11	Node 2	24.655
	Node 13	Node 8	25.642
	Node 23	Node 9	13.334
Fuel cell	Node 8	Node 15	10.801

independently, without considering the coupling between hydrogen and electrical energy.

Scenario 3: Collaborative planning of the PN and HN, but only hydrogen fuel cell units are configured on the hydrogen-electricity hybrid equipment, creating a one-way coupling between hydrogen and electrical energy.

4.2.2. Comparison of planning results

Through the collaborative planning method based on the improved Benders hybrid tabu search algorithm, the results of equipment siting and capacity under scenario 1 are obtained, as shown in Table 9. The

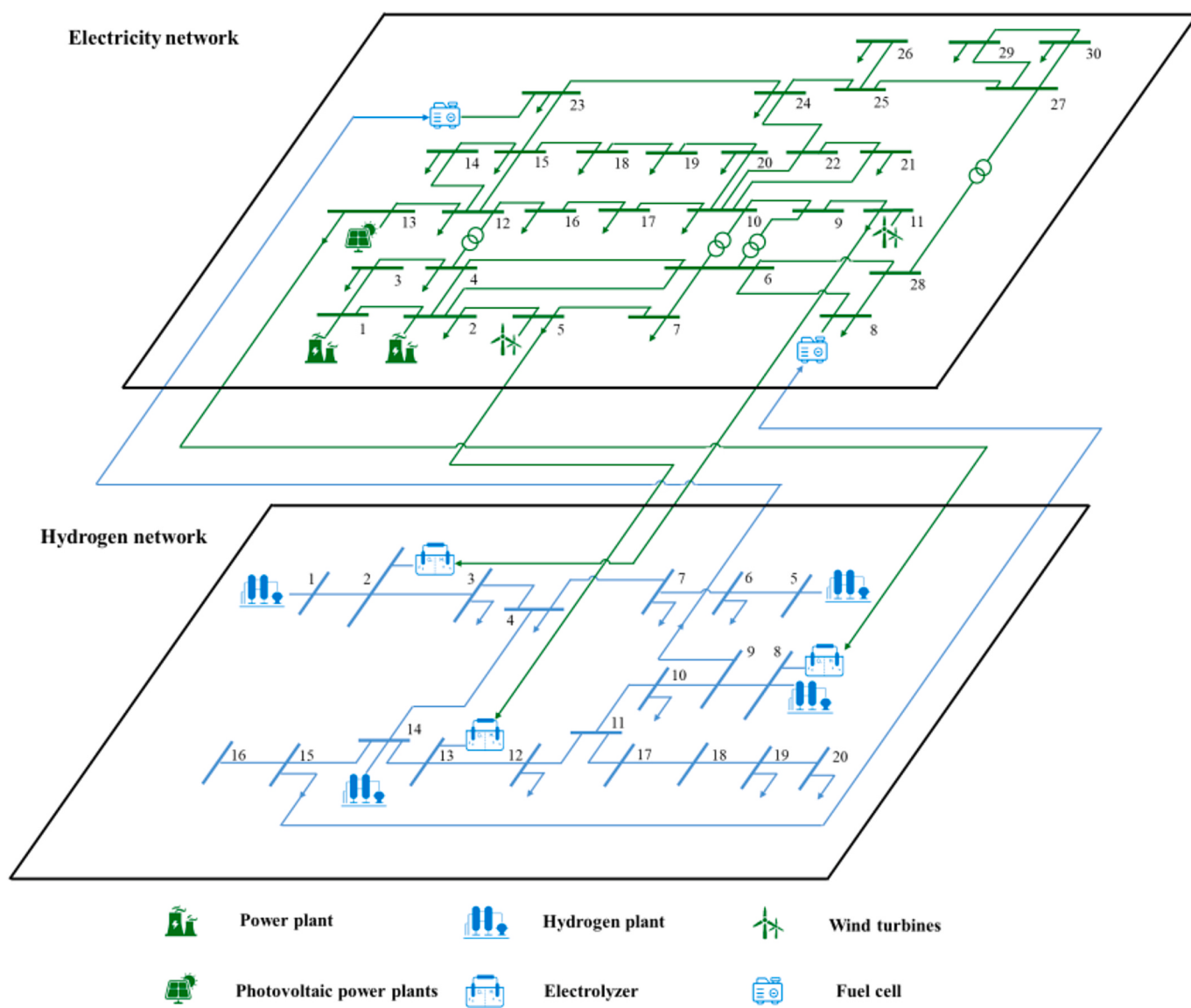


Fig. 10. Topology of PN and HN after collaborative planning.

Table 10
Planning result under Scenario 2.

Planned equipment	Node	Capacity (MW)
Wind turbines	Node 5	27.850
	Node 11	95.751
Photovoltaic panels	Node 8	54.688
	Node 13	96.489

Table 11
Planning result under Scenario 3.

Planned equipment	Node		Capacity (MW)
	PN	HN	
Wind turbines	Node 5	–	15.469
	Node 13	–	23.419
Photovoltaic panels	Node 8	–	42.417
Fuel cell	Node 19	Node 15	21.743
	Node 23	Node 9	33.870

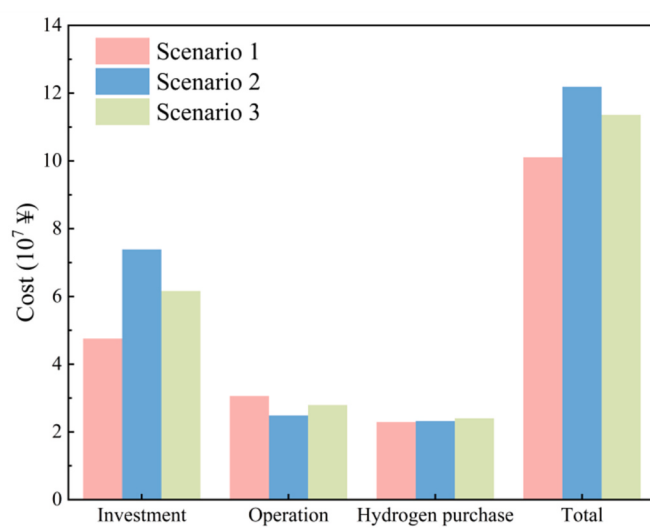


Fig. 11. Cost in different scenarios.

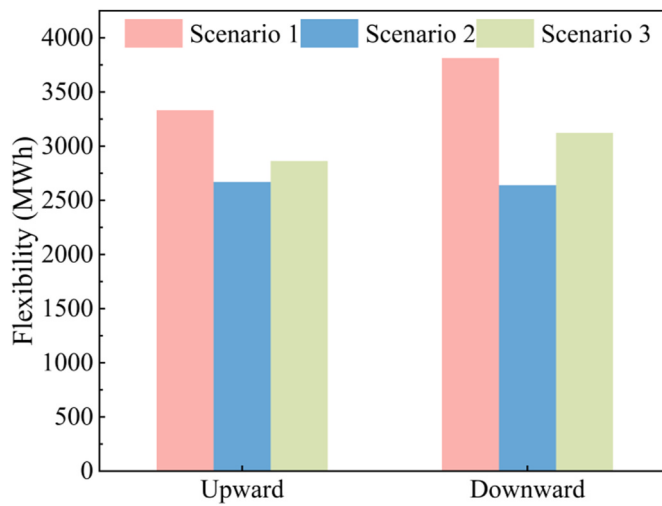


Fig. 12. Flexibility in different scenarios.

the lowest, at 2.292×10^7 ¥.

4.2.3. Analysis of operation optimization result

Flexibility is essentially the ability of a system to regulate in response to uncertainty, which is generally caused by renewable energy sources and load fluctuations. All equipment with power adjustment capability is considered a flexibility resource, which in this paper includes power plant, hydrogen plant, electrolyzer, fuel cell. The flexibility has two orientations: upward and downward. The operation flexibility of the system is calculated as follows [45].

$$F_{\text{up}} = \sum_{t=1}^{t_{\max}} \sum_{eq=1}^{eq_{\max}} \min(r_{eq,\text{adj}}, P_{eq,\text{max}} - P_{eq,t}) \quad (57)$$

$$F_{\text{down}} = \sum_{t=1}^{t_{\max}} \sum_{eq=1}^{eq_{\max}} \min(r_{eq,\text{adj}}, P_{eq,t} - P_{eq,\text{min}}) \quad (58)$$

where F_{up} and F_{down} are flexibility in the upward/downward direction,

respectively. $P_{eq,\text{max}}$ and $P_{eq,\text{min}}$ are the maximum and minimum output power of the equipment, respectively. $P_{eq,t}$ is the output power of the equipment at moment t . $r_{eq,\text{adj}}$ is the power adjustment limit of the equipment.

Based on the operation results obtained from the optimization, the flexibility of the three scenarios is calculated, as shown in Fig. 12. The flexibility in the upward direction for Scenario 1 is 3331.6 MWh, which is an improvement of 24.8 % (661.6 MWh) and 16.4 % (468.8 MWh) relative to Scenario 2 and Scenario 3, respectively. The flexibility in the downward direction for Scenario 1 is 3814.2 MWh, an improvement of 44.5 % (1174.2 MWh) and 22.2 % (692.2 MWh) relative to Scenario 2 and Scenario 3, respectively. This is due to the fact that in Scenario 1, the PN and the HN are planned collaboratively, and the electrolyzer and the fuel cell are able to flexibly adjust their operation strategies, thus increasing the overall system flexibility. Scenario 2 can only rely on power plants and hydrogen plants, and flexibility is greatly limited. Scenario 1 forms a completed electric-hydrogen-electric closed loop relative to Scenario 3. The reason that the flexibility in the upward direction is less than the flexibility in the downward direction is that both the electrolyzer and the fuel cell equipment are operated at higher loads. In summary, electricity-hydrogen collaboration is able to respond more efficiently and flexibly to power uplift demands on the grid, such as sudden load increases or renewable energy output shortfalls, and has a greater ability to consume excess renewable energy.

The operation characteristics of the equipment, PN and HN in Scenario 1 are described next. The operation output of the power plants located at node 1 and 2, and the fuel cell at node 23 and 8 of the PN on a typical day is shown in Fig. 13. The power plants play a vital role in the supply of electrical energy, while the fuel cell provide supplementary energy for the shortfall loads in the PN. Among them, the power plant at node 1, whose installed capacity has been preset to 200 MW, has a maximum output of 132.2 MW during actual operation, which indicates that it is not operating at full load. Therefore, during the planning stage of the system, if the original power plants are also included in the planning, the investment cost of the system can be reduced by reasonably adjusting their installed capacity under the premise of ensuring a stable supply of electric power. The hydrogen fuel cell at node 23 and node 8 also play a key role in the PN, as they are able to provide the necessary supplemental power immediately during the peak demand

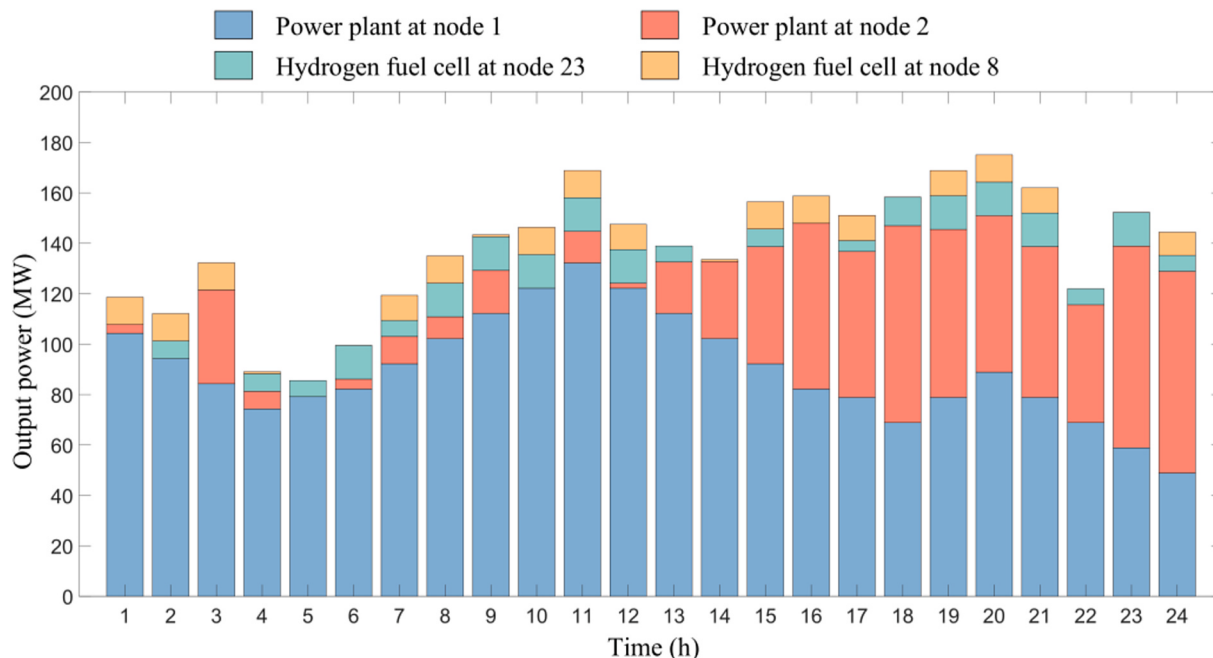
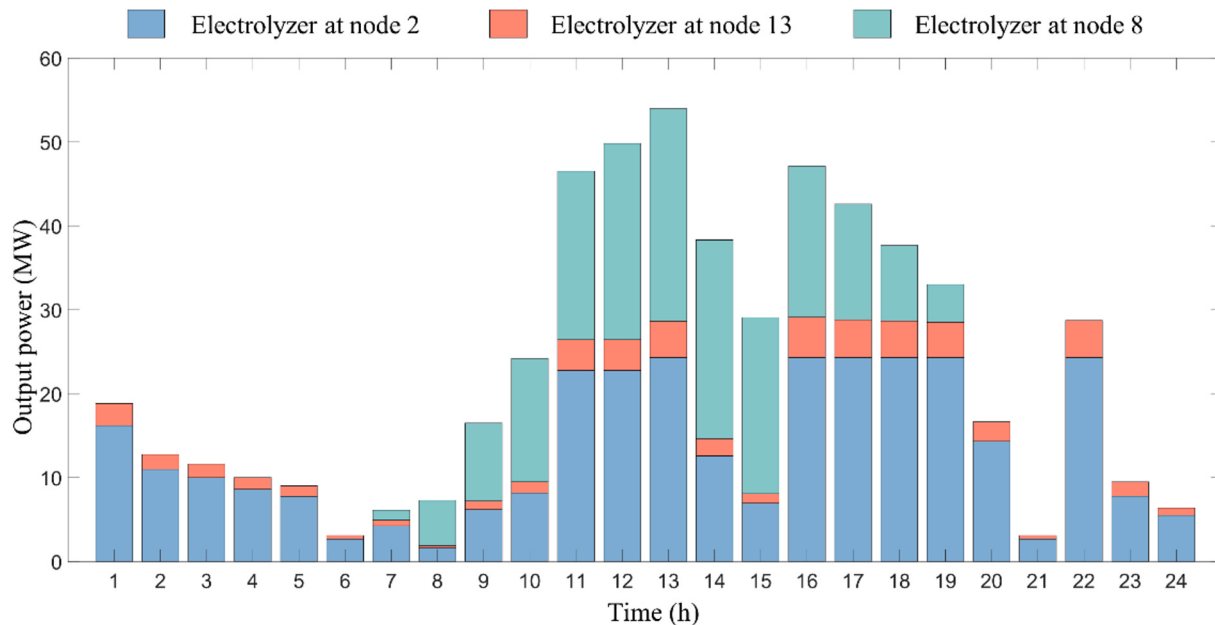
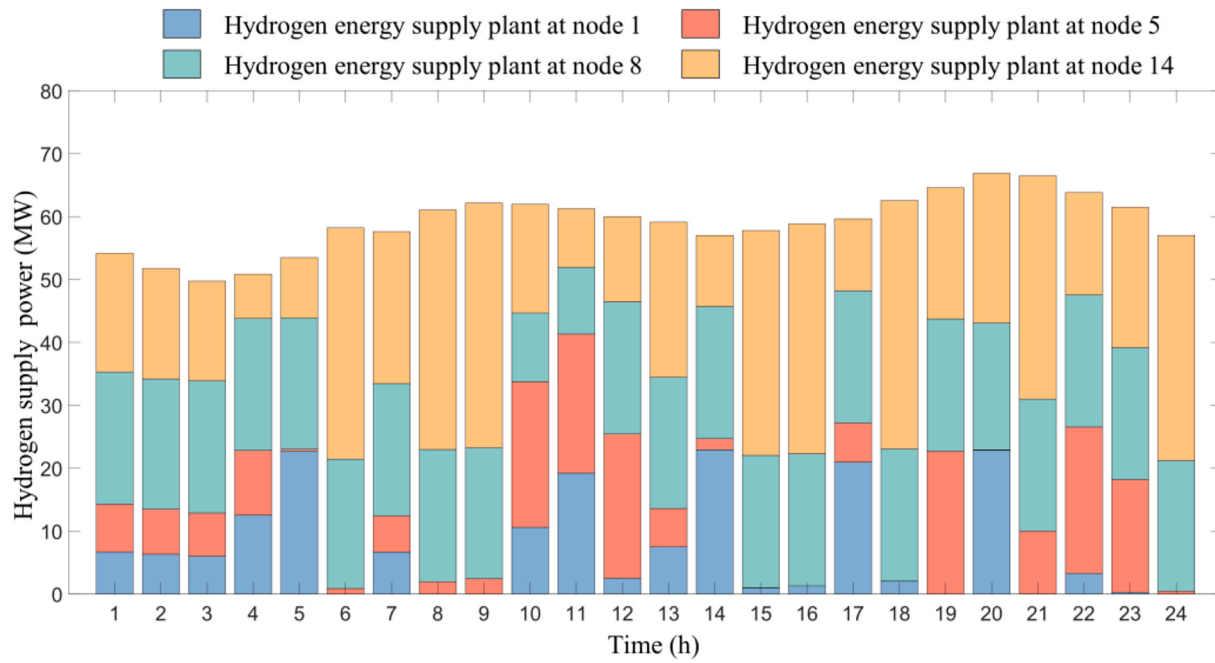


Fig. 13. Output of generating units.

**Fig. 14.** Output of the electrolyzer.**Fig. 15.** Output of the hydrogen energy supply station.

hours, effectively mitigating the fluctuation in the output of the power plants and ensuring the stability of the power supply. This peaking capability improves the operational flexibility of the system, enabling the system to respond more effectively to different load demands. In addition, the fuel cell units are able to maintain a high equipment utilization rate in most of the time, providing stable power output to the PN, which further verify the rationality of the capacity planning.

The output characteristics of the electrolyzer at node 2, node 13 and node 8 in the HN on a typical day are depicted in Fig. 14. It can be observed that when the output of each generation equipment in the electric PN sufficiently meets the electric load demand, while the renewable energy generation has not been fully consumed, the system is able to convert the surplus electric energy into hydrogen through the

electrolyzer and deliver it to the hydrogen load nodes in the HN. It should be noted that the electrolyzer at node 8 of the HN does not produce power during the night due to the fact that the operation strategy of the electrolyzer is set in the planning to obtain its input power only from renewable energy generation equipment.

The operational characteristic of the hydrogen energy supply plant station at node 1, node 5, node 8 and node 14 in the HN is demonstrated in Fig. 15. The hydrogen supply capacity of each hydrogen energy supply station basically meets the hydrogen load demand of the system. The system will correspondingly reduce the amount of external hydrogen purchase during the peak period of the equipment output of each electrolyzer, thus reducing the hydrogen purchase cost, and the economy of the system are improved.

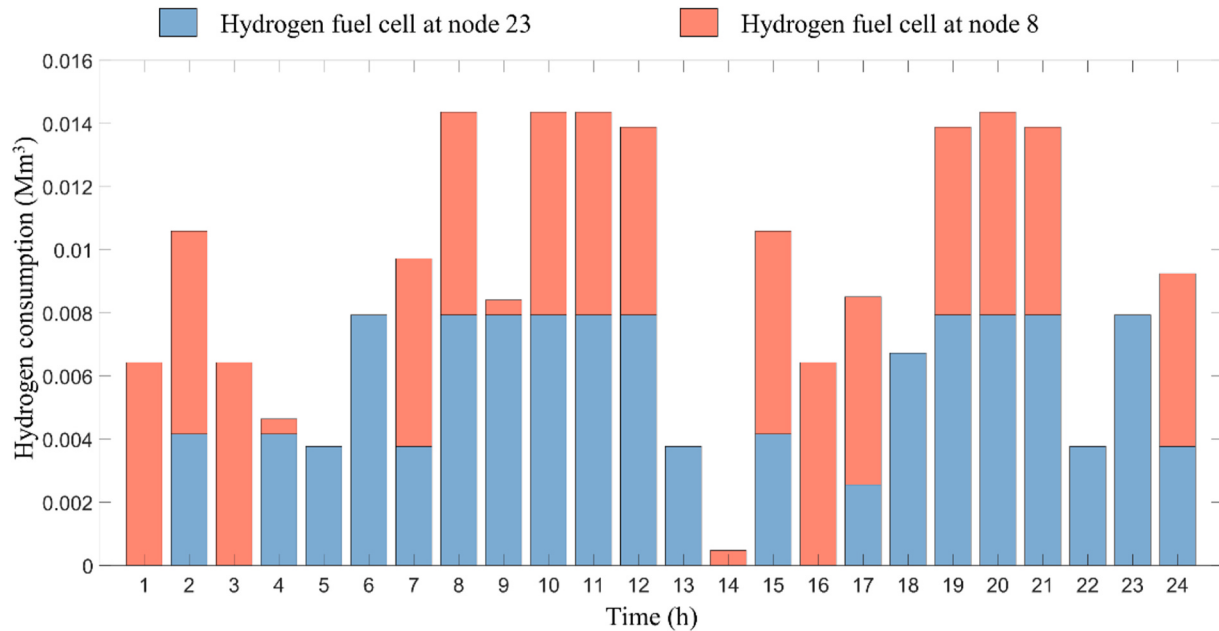


Fig. 16. Hydrogen consumption of hydrogen fuel cell units.

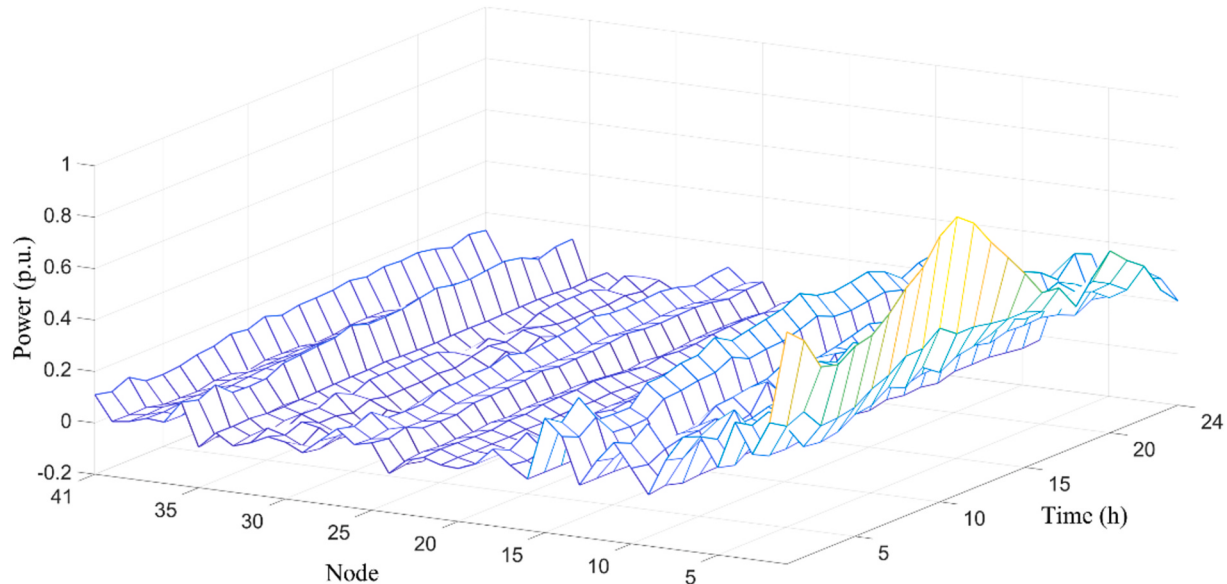


Fig. 17. The variation of branch power in the PN.

The hydrogen consumption of the hydrogen fuel cell units at PN node 23 and node 8 on a typical day is shown in Fig. 16. It is found that the hydrogen fuel cell units are able to maintain a high equipment utilization rate at most of the time, which plays a key role in maintaining the balance between the supply and demand of hydrogen and electricity in the system. At 08:00, 10:00, 11:00 and 20:00 on a typical day, the hydrogen fuel cell units at both nodes are operated at full capacity, which was due to the fact that the hydrogen load of the system is fully satisfied during these hours, while the electric energy supply of the system is relatively insufficient. To cope with this situation, the system coordinates the supply of hydrogen and electricity by increasing the output of the hydrogen fuel cell units, which in turn improves the operational flexibility of the PN and HN.

The power changes of 41 branches of the IEEE 30-node system on a typical day are depicted in Fig. 17. The transmitted power of branch 1 and branch 2 is significantly higher than that of the other branches, and

the power change trend of branch 1 is consistent with the change of the output of the power plant at node 1. This is due to the fact that both branch 1 and branch 2 are directly connected to the 200 MW power plant located at node 1 of the PN, which is the main energy supply equipment of the entire PN, and thus the branch connected to it bears a higher transmission power. In the actual system planning, it can be considered to add transmission lines in the corresponding branch location, so as to effectively disperse the power load, in order to avoid power overloading of the line, and guarantee the energy supply reliability of the system.

Figs. 18 and 19 show the changes in pressure and pipeline gas flow at each node of the 20-node HN on a typical day, respectively. It can be analyzed that the HN node 1 shows more obvious pressure fluctuation at 5:00, 11:00, 14:00, 17:00 and 20:00, and these fluctuating moments are closely related to the full-load operation status of the hydrogen supply plant station, and the output shows a larger change at these times. At the

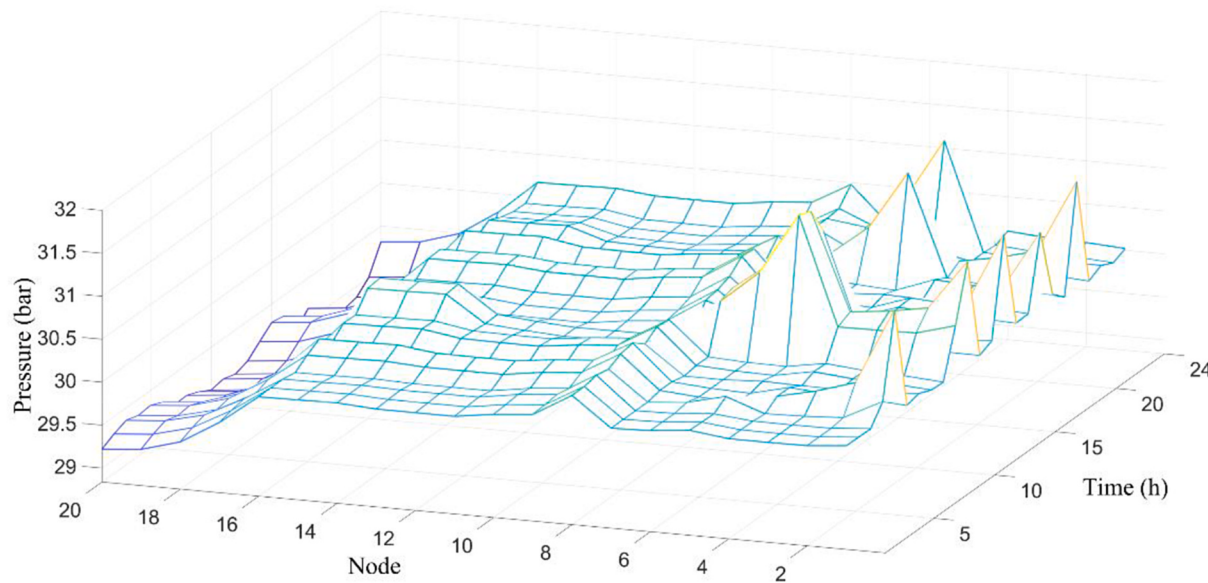


Fig. 18. Variation of node pressure in HN.

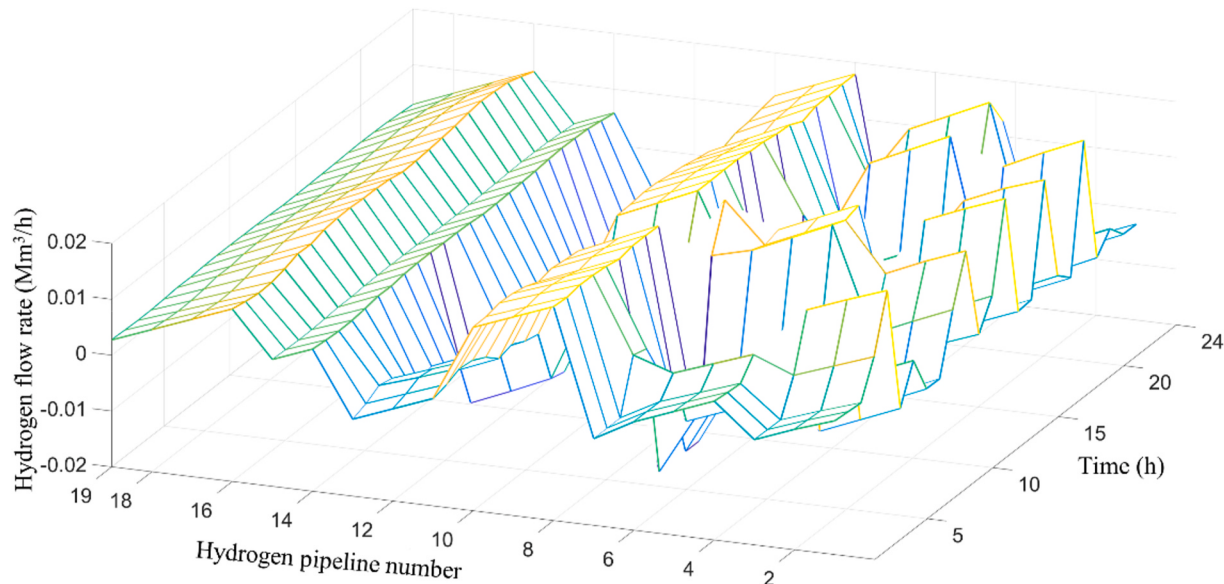


Fig. 19. The pipeline gas flow variation in the HN.

same time, the hydrogen flow in the hydrogen pipeline 1 directly connected to node 1 shows a consistent trend with the air pressure fluctuation at node 1, which indicates that the operating state of the hydrogen energy supply plant at this node directly affects the hydrogen flow in the pipeline connected to it. Similarly, there is an obvious consistency between the trend of the pressure change at node 5 and the output of its hydrogen energy supply plant station, and the change in the hydrogen flow in pipeline 4 is also consistent with the change in the pressure at node 5, which further verifies the correlation between the output of the hydrogen energy supply plant station and the change in the air flow and pressure in the HN.

In summary, the proposed collaborative planning scheme for the PN and HN fully realizes the operation flexibility of each equipment. By analyzing the operation characteristics of the PN and HN, it can be seen that these networks operate stably within a reasonable range, which indicates the reasonableness and effectiveness of the planning.

4.2.4. Sensitivity analysis

The sensitivity analysis of the two constraints, renewable energy penetration and energy supply reliability, is performed in this section, and the results are shown in Fig. 20. The baseline for the study is a renewable energy penetration of 35 % and an energy supply reliability of 100 % in Scenario 1. As both renewable energy penetration and energy supply reliability increase, costs increase, due to the need to deploy more turbines and PV. The difference is that an average 10 % increase in renewable energy penetration results in an average cost increase of 32.4 %, while an average 10 % increase in energy supply reliability results in an average cost increase of 25.9 %. In addition, the slope of Fig. 20 (a) becomes progressively larger with increasing renewable energy penetration, indicating that more inputs are required. The study proposes treating high energy supply reliability as a rigid constraint while considering high renewable energy penetration as a flexible constraint in system planning. It is recommended that energy supply reliability be prioritized in energy system planning and that renewable energy

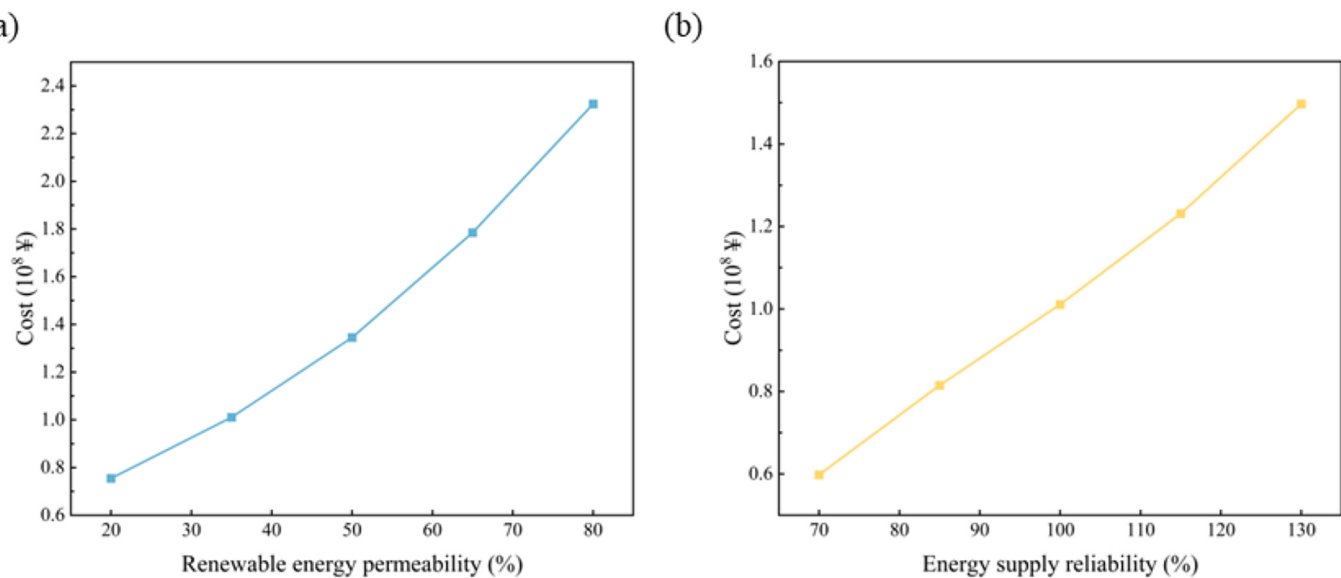


Fig. 20. Sensitivity analysis. (a) Renewable energy permeability. (b) Energy supply reliability.

penetration be increased in a phased manner.

5. Conclusion

Collaborative planning for the PN and HN is investigated in this paper. The dynamic model of hydrogen pipeline network and the power flow model of PN is constructed, and the improved Benders combined tabu search algorithm is adopted to solve the collaborative planning problem. Through the IEEE 5-node system and 7-node hydrogen system case study, the results indicate that compared to steady state modeling, considering the slow dynamics of the hydrogen pipeline and the pipe storage characteristics during planning results in a reduction of 1.128 MW (31.7 %) in the capacity of the hydrogen storage tanks, which improves the economics of the planning scheme to a certain extent. Through the IEEE 30-node system and 20-node hydrogen system case study, the research indicates that the total cost of the collaboratively planned the PN and HN is reduced by 17.06 %, with a reduction in the annual investment cost and the annual hydrogen purchase cost, but an increase in the annual operation cost, compared to the separate planning. The analysis of the operation results on a typical day shows that both the PN and HN operate stably within a reasonable range, verifying the rationality of the planning scheme and the effectiveness of the collaborative planning method. In addition, the flexibility in the upward and downward directions of the PN and HN collaborative planning is increased by 24.8 % and 44.5 %, respectively. And the coordination and complementarity of the various types of equipment demonstrates the high degree of operation flexibility.

To promote the collaborative planning of the PN and HN, governments should develop and publish a clear hydrogen development roadmap, ensuring its close alignment with PN planning. For instance, setting phased targets for hydrogen production and distribution, while coordinating these with renewable energy development goals. Additionally, governments can promote the implementation of shared investment models or revenue-sharing agreements to equitably distribute costs and benefits, ensuring a balance among the needs of different stakeholders and encouraging active participation from various enterprises in the collaborative planning process.

Future research can explore the application of collaborative planning models to real-world large scale energy systems, such as urban power grids, hydrogen supply networks, and transportation networks. Large-scale energy systems typically consist of multiple interconnected subsystems and face various uncertainties, such as fluctuations in renewable

energy generation, dynamic changes in energy demand, and adjustments in policy environments. To enhance the adaptability of planning models to uncertainties, future research could integrate stochastic optimization or robust optimization methods, taking into account the maximum possible load fluctuations and extreme scenarios. This would ensure that the planned systems can maintain efficient and reliable operation under uncertain conditions.

CRediT authorship contribution statement

Guangyao Fan: Writing – review & editing, Writing – original draft, Software, Methodology, Investigation, Data curation. **Wenchuan Zhang:** Writing – review & editing, Data curation. **Haozeng Bie:** Writing – review & editing. **Xing Dong:** Writing – review & editing. **Ruicheng He:** Writing – original draft, Software. **Hui Zhang:** Software. **Fan Li:** Writing – review & editing. **Bo Sun:** Writing – review & editing, Project administration, Funding acquisition. **Fengwen Pan:** Writing – review & editing, Funding acquisition.

Declaration of competing interest

The authors declare that they have no known competing financial interests or personal relationships that could have appeared to influence the work reported in this paper.

Acknowledgement

This research has been supported by the National Key R&D Program of China (grant number: 2022YFB4004401) and the Major Program of National Natural Science Foundation of China (grant number: 62192753).

Appendix A. Supplementary data

Supplementary data to this article can be found online at <https://doi.org/10.1016/j.ijhydene.2025.04.038>.

References

- [1] Yang X, Nielsen CP, Song S, McElroy MB. Breaking the hard-to-abate bottleneck in China's path to carbon neutrality with clean hydrogen. *Nat Energy* 2022;7:955–65.
- [2] Medium and long-term plan for the development of the hydrogen energy industry (2021–2035). 2022.

- [3] Song S, Lin H, Sherman P, Yang X, Nielsen CP, Chen X, et al. Production of hydrogen from offshore wind in China and cost-competitive supply to Japan. *Nat Commun* 2021;12.
- [4] Zeng R, Tang XL, Deng Y, Zhang XF, Li HQ, Yin W, et al. Design and optimization of solar energy system with hydrogen energy storage and alkaline fuel cell. *Energy Convers Manag* 2023;295.
- [5] Li M, Ming P, Huo R, Mu H. Economic assessment and comparative analysis of hydrogen transportation with various technical processes. *J Renew Sustain Energy* 2023;15.
- [6] Paul S, Poudyal A, Poudel S, Dubey A, Wang Z. Resilience assessment and planning in power distribution systems: past and future considerations. *Renew Sustain Energy Rev* 2024;189.
- [7] Flores-Quiroz A, Strunz K. A distributed computing framework for multi-stage stochastic planning of renewable power systems with energy storage as flexibility option. *Appl Energy* 2021;291.
- [8] Zhang H, Liao K, Yang J, Zheng S, He Z. Frequency-constrained expansion planning for wind and photovoltaic power in wind-photovoltaic-hydro-thermal multi-power system. *Appl Energy* 2024;356.
- [9] Li X, Wu X, Gui D, Hua Y, Guo P. Power system planning based on CSP-CHP system to integrate variable renewable energy. *Energy* 2021;232.
- [10] Zhang Z, Guo Z, Zhou M, Wu Z, Yuan B, Chen Y, et al. Equalizing multi-temporal scale adequacy for low carbon power systems by co-planning short-term and seasonal energy storage. *J Energy Storage* 2024;84.
- [11] Halloran C, Lizana J, Fele F, McCulloch M. Data-based, high spatiotemporal resolution heat pump demand for power system planning. *Appl Energy* 2024;355.
- [12] Maulén L, Castro M, Lorca Á, Negrete-Pincetic M. Optimization-based expansion planning for power and hydrogen systems with feedback from a unit commitment model. *Appl Energy* 2023;343.
- [13] Carmona R, Miranda R, Rodriguez P, Garrido R, Serafini D, Rodriguez A, et al. Assessment of the green hydrogen value chain in cases of the local industry in Chile applying an optimization model. *Energy* 2024;300.
- [14] Li J, Liu C, Kang B, Ma T. Research on coupling coordination and spatial-temporal evolution of hydrogen energy industry in hebei province based on R-P-D chain. *Int J Hydrogen Energy* 2024;79:1180–90.
- [15] Khaligh V, Ghezelbash A, Liu J, Won W, Koo J, Na J. Multi-period hydrogen supply chain planning for advancing hydrogen transition roadmaps. *Renew Sustain Energy Rev* 2024;200.
- [16] Zhou Y, Qin X, Mei W, Yang W, Ni M. Multi-period urban hydrogen refueling stations site selection and capacity planning with many-objective optimization for hydrogen supply chain. *Int J Hydrogen Energy* 2024;79:1427–41.
- [17] Zhou Y, Ge J, Li X, Zang H, Chen S, Sun G, et al. Bi-level distributionally robust optimization model for low-carbon planning of integrated electricity and heat systems. *Energy* 2024;302.
- [18] Safari A, Farrokhfaf M, Shahsavari H, Hosseinezhad V. Stochastic planning of integrated power and natural gas networks with simplified system frequency constraints. *Int J Elec Power* 2021;132.
- [19] Sun GQ, Chen S, Wei ZN, Cheung KW, Zang HX. Corrective security-constrained optimal power and gas flow with binding contingency identification. *Ieee T Sustain Energ* 2020;11:1033–42.
- [20] Wang Y, Yang Y, Xu Q. Integrated planning of power-gas systems considering N-1 constraint. *Energy Rep* 2023;9:1274–81.
- [21] Qiu Y, Li Q, Li S, Deng Q, Chen W, Benbouzid M, et al. Lifecycle collaborative planning for traction power supply systems with integrated energy access. *IEEE Transactions on Transportation Electrification* 2025;11:5055–68.
- [22] Li J, Lin J, Song Y, Xiao J, Liu F, Zhao Y, et al. Coordinated planning of HVDCs and power-to-hydrogen supply chains for interregional renewable energy utilization. *Ieee T Sustain Energ* 2022;13:1913–29.
- [23] Jiang H, Qi B, Du E, Zhang N, Yang X, Yang F, et al. Modeling hydrogen supply chain in renewable electric energy system planning. *IEEE Trans Ind Appl* 2022;58:2780–91.
- [24] Pu Y, Li Q, Luo S, Chen W, Breaz E, Gao F. Peer-to-Peer electricity-hydrogen trading among integrated energy systems considering hydrogen delivery and transportation. *Ieee T Power Syst* 2024;39:3895–911.
- [25] Sun Q, Wu Z, Gu W, Liu P, Wang J, Lu Y, et al. Multi-stage Co-planning model for power distribution system and hydrogen energy system under uncertainties. *J Modern Power Syst Clean Energy* 2023;11:80–93.
- [26] Yang T, Geng Y, Wang H. Dynamic energy flow optimization of electricity and hydrogen-enriched natural gas integrated energy systems. *Int J Hydrogen Energy* 2025;109:1274–85.
- [27] Li JW, Yang LM, Yang QQ, Wei ZB, He YT, Lan H. Degradation adaptive energy management with a recognition-prediction method and lifetime competition-cooperation control for fuel cell hybrid bus. *Energy Convers Manag* 2022;271.
- [28] Liu S, Zhou J, Liang G, Du P, Li Z, Li C. Optimizing large-scale hydrogen storage: a novel hybrid genetic algorithm approach for efficient pipeline network design. *Int J Hydrogen Energy* 2024;66:430–44.
- [29] Gan W, Yan M, Yao W, Guo J, Fang J, Ai X, et al. Multi-network coordinated hydrogen supply infrastructure planning for the integration of hydrogen vehicles and renewable energy. *IEEE Trans Ind Appl* 2022;58:2875–86.
- [30] Wang C, Chen S, Zhao JT, Zhou YZ, Wei ZN, Zheng S. Coordinated scheduling of integrated electricity, heat, and hydrogen systems considering energy storage in heat and hydrogen pipelines. *J Energy Storage* 2024;85.
- [31] Shchetinin D, Knezovic K, Oudalov A. Pipeline dynamics approximation for coordinated planning of power and hydrogen systems. *Sustain Energy Grids Networks* 2023;33.
- [32] Wang C, Liu C, Chen J, Zhang G. Cooperative planning of renewable energy generation and multi-timescale flexible resources in active distribution networks. *Appl Energy* 2024;356.
- [33] Zhao ZY, Wang ZS, Hao JH, Wang SJ, Wang XC, Xie H, et al. A multi-objective power flow optimization model of electric and thermal distribution network using the power flow method. 2022 9th international forum on electrical engineering and automation. Ifeea; 2022. p. 687–90.
- [34] Yin W, Qin X, Huang Z. Optimal dispatching of large-scale electric vehicles into grid based on improved second-order cone. *Energy* 2022;254.
- [35] Nastasi B, Mazzoni S, Groppi D, Romagnoli A, Astiaso Garcia D. Optimized integration of Hydrogen technologies in Island energy systems. *Renew Energy* 2021;174:850–64.
- [36] Yuan Y, Ding T, Chang X, Jia W, Xue Y. A distributed multi-objective optimization method for scheduling of integrated electricity and hydrogen systems. *Appl Energy* 2024;355.
- [37] Fan G, Yu B, Sun B, Li F. Multi-time-space scale optimization for a hydrogen-based regional multi-energy system. *Appl Energy* 2024;371.
- [38] Tao Y, Qiu J, Lai S, Zhao J. Integrated electricity and hydrogen energy sharing in coupled energy systems. *Ieee T Smart Grid* 2021;12:1149–62.
- [39] Zhang J, Liu J, Chen L, Zhang L, Zeng P, Li Y. Reliability evaluation of high permeability renewable energy distribution network considering energy storage charge and discharge strategy. *Energy Rep* 2023;9:361–8.
- [40] Jahannoosh M, Nowdeh SA, Naderipour A, Kamayab H, Davoudkhani IF, Klemes JJ. New hybrid meta-heuristic algorithm for reliable and cost-effective designing of photovoltaic/wind/fuel cell energy system considering load interruption probability. *J Clean Prod* 2021;278.
- [41] Liu JH, Xu ZB, Wu J, Liu K, Sun XH, Guan XH. Optimal planning of internet data centers decarbonized by hydrogen-water-based energy systems. *Ieee T Autom Sci Eng* 2023;20:1577–90.
- [42] Kumar RP, Karthikeyan G. A multi-objective optimization solution for distributed generation energy management in microgrids with hybrid energy sources and battery storage system. *J Energy Storage* 2024;75.
- [43] Liu J, Xu Z, Wu J, Liu K, Guan X. Optimal planning of distributed hydrogen-based multi-energy systems. *Appl Energy* 2021;281.
- [44] Petkov I, Gabrielli P. Power-to-hydrogen as seasonal energy storage: an uncertainty analysis for optimal design of low-carbon multi-energy systems. *Appl Energy* 2020;274.
- [45] Zhang YM, Li JR, Ji XQ, Yang M, Ye PF. Optimal scheduling of electricity-gas-heat integrated energy system with coordination of flexibility and reliability. *Sustain Energy Technn* 2024;71.